

35 **ABSTRACT**

36 Here we present the experimental design and results from a new mid-Pliocene simulation using the
37 latest version of the UK's physical climate model, HadGEM3-GC31-LL, conducted under the
38 auspices of CMIP6/PMIP4/PlioMIP2. Although two other paleoclimate simulations have been
39 recently run using this model, they both focused on more recent periods within the Quaternary and
40 therefore this is the first time this version of the UK model has been run this far back in time. The
41 mid-Pliocene Warm Period, ~3 Ma, is of particular interest because it represents a time period when
42 the Earth was in equilibrium with CO₂ concentrations roughly equivalent to those of today, providing
43 a possible analogue for current and future climate change.

44

45 The implementation of the Pliocene boundary conditions is firstly described in detail, based on the
46 PRISM4 dataset, including CO₂, ozone, orography, ice mask, lakes, vegetation fractions and
47 vegetation functional types. These were incrementally added into the model, to change from a
48 preindustrial setup to a Pliocene setup.

49

50 The results of the simulation are then presented, which are firstly compared with the model's pre-
51 industrial simulation, secondly with previous versions of the same model and with available proxy
52 data, and thirdly with all other models included in PlioMIP2. Firstly, the comparison with
53 preindustrial suggests that the Pliocene simulation is consistent with current understanding and
54 existing work, showing warmer and wetter conditions, and with the greatest warming occurring over
55 high latitude and polar regions. The global mean surface air temperature anomaly at the end of the
56 Pliocene simulation is 5.1°C, which is the 2nd highest of all models included in PlioMIP2 and is
57 consistent with the fact that HadGEM3-GC31-LL has one of the highest Effective Climate
58 Sensitivities of all CMIP6 models. Secondly, the comparison with previous generation models and
59 with proxy data suggests a clear increase in global sea surface temperatures as the model has
60 undergone development. Up to a certain level of warming, this results in a better agreement with
61 available proxy data, and the "sweet spot" appears to be the previous CMIP5 generation of the model,
62 HadGEM2-AO. The most recent simulation presented here, however, appears to show poorer
63 agreement with the proxy data compared with HadGEM2, and may be overly sensitive to the Pliocene
64 boundary conditions resulting in a climate that is too warm. Thirdly, the comparison with other
65 models from PlioMIP2 further supports this conclusion, with HadGEM3-GC31-LL being one of the
66 warmest and wettest models in all of PlioMIP2 and, if all the models are ordered according to
67 agreement with proxy data, HadGEM3-GC31-LL ranks approximately halfway among them. A
68 caveat to these results is the relatively short run length of the simulation, meaning the model is not in
69 full equilibrium. Given the computational cost of the model it was not possible to run for longer; a
70 Gregory plot analysis indicates that had it been allowed to come to full equilibrium, the final global
71 mean surface temperature could have been approximately 1.5°C higher.

72 1. INTRODUCTION

73 Model simulations of past climate states are useful because, among other aspects, they allow us to
74 interrogate the mechanisms that have caused past climate change (Haywood *et al.* 2020, Lunt *et al.*
75 2021). They also give us a global picture of past climate variables (such as sea surface temperature,
76 SST) that can only be reconstructed by geological data at specific locations, and of variables (such as
77 upper atmospheric winds) that cannot be reconstructed by geological data at all. However, before
78 models can be used in this way, it is important to validate them by comparing with geological data,
79 where available, from the time periods of interest. Such model-data comparisons can also be useful
80 for evaluating the model outside of the modern climate states that it was likely tuned to, thereby
81 providing an independent assessment of the model that can be important for interpreting any future
82 climate projections arising from the model (e.g. Zhu *et al.* 2020).

83

84 The mid-Pliocene Warm Period (mPWP, ~3 million years ago, hereafter referred to as the Pliocene) is
85 an ideal climate state for such a model-data comparison because: i) there has recently been a
86 concerted community effort to provide a synthesis of proxy SST reconstructions (McClymont *et al.*
87 2020); ii) community-endorsed boundary conditions exist which can be used to configure climate
88 model simulations (Haywood *et al.* 2016); and iii) there is a wealth of previous model
89 intercomparison projects (MIPs), with which model simulations can be compared and contrasted, that
90 have been carried out with these recent boundary conditions (PlioMIP2, Dowsett *et al.* 2016 and
91 Haywood *et al.* 2020) and with previous versions of the boundary conditions (PlioMIP1, Haywood *et al.*
92 *et al.* 2013). The Pliocene is also a relatively warm period compared to both preindustrial conditions
93 and those of today, with comparable CO₂ levels to today (McClymont *et al.* 2020, Salzmann *et al.*
94 2013), and so provides a climate state with similarities to those that might be expected in the future
95 (Burke *et al.* 2018, Tierney *et al.* 2020).

96

97 PlioMIP2 was a community effort to carry out and analyse coordinated model simulations to explore
98 mechanisms associated with Pliocene climate, and to evaluate multiple models with Pliocene proxy
99 data. To date, 16 models have participated in PlioMIP2, all of which used boundary conditions from
100 the US Geological Survey's PRISM4 (Pliocene Research, Interpretation and Synoptic Mapping v4;
101 see Dowsett *et al.* 2016) and the results of this intercomparison and evaluation are described in
102 Haywood *et al.* 2020 (hereafter abbreviated to H20). H20 first explored the large-scale features
103 (global means, polar amplification and land-sea contrast) of temperature and precipitation in the
104 simulations, finding a global ensemble mean warming of 3.2°C relative to preindustrial and a 7%
105 increase in precipitation. There was a clear signal of polar amplification, but tropical zonal gradients
106 remained largely unchanged compared with preindustrial. Compared with proxies from Foley and
107 Dowsett (2019), the SSTs in the tropics were broadly consistent in the models and data, and in the
108 Atlantic the polar amplification was better represented by the models compared with previous model-

109 data comparisons such as those from PlioMIP1. Recent studies using the PlioMIP2 ensemble have
110 explored other aspects of the model simulations, such as ocean circulation (Zhang *et al.* 2021) and the
111 African monsoon (Berntell *et al.*, in review). It is of interest to evaluate simulations from additional
112 models as they become available, and that is what we do here, presenting results from a new model,
113 HadGEM3-GC31-LL, for the Pliocene. This is of particular interest because HadGEM3-GC31-LL is
114 a Coupled Model Intercomparison Project Phase 6 (CMIP6) “high Effective Climate Sensitivity
115 (ECS)” model (Zelinka *et al.* 2020), with a climate sensitivity to CO₂ doubling of more than 5°C
116 (Andrews *et al.* 2019). Only one other model in CMIP6, CanESM5, has a higher climate sensitivity
117 (5.64°C compared with 5.55°C). HadGEM3-GC31-LL is also of interest because it represents the
118 third generation of UK Met Office model that has participated in PlioMIP (Bragg *et al.* 2012, Tindall
119 and Haywood 2020, Hunter *et al.* 2019), allowing us to assess how much, if any, progress has been
120 made in simulating the Pliocene with the UK family of models.

121

122 In this paper we address 3 main questions:

- 123 1) What are the large-scale features of the Pliocene climate produced by HadGEM3-GC31-LL?
- 124 2) To what extent has the development of new boundary conditions and more complex models
125 led to improvements in the simulation of the Pliocene by UK Met Office models?
- 126 3) How does HadGEM3-GC31-LL compare with other models participating in PlioMIP2?

127

128 Section 2 of this paper describes HadGEM3-GC31-LL, how the PlioMIP2 boundary conditions were
129 implemented in the model, and the experimental design of the model. Section 3 presents the large-
130 scale features of the Pliocene in HadGEM3-GC31-LL, and Section 4 compares the HadGEM3-GC31-
131 LL simulation with proxy data and previous generations of the same UK model, and with other
132 PlioMIP2 models.

133

134 **2. MODEL AND EXPERIMENT DESIGN**

135 **2.1. Naming conventions and terminology**

136 Consistent with CMIP nomenclature, when the simulation is spinning up towards atmospheric and
137 oceanic equilibrium, with initially incomplete boundary conditions, it is referred to as the ‘Spin-up
138 phase’ and is only briefly presented here. In contrast, once all required boundary conditions were
139 implemented, the results themselves are taken from the end of the simulation, referred to here as the
140 ‘Production run’. Here, results are based on the final 50-year climatology of this production run.
141 Concerning geological intervals, the preindustrial and mid-Pliocene Warm Period are referred to as
142 the PI and Pliocene, respectively. In contrast, concerning the model simulations using HadGEM3-
143 GC31-LL, consistent with CMIP6 they are referred to as the *piControl* and *mPWP* simulations,
144 respectively. We also make use of the naming convention of Haywood *et al.* 2016, hereafter
145 abbreviated to H16), including the nomenclature Ex^c (where c is the concentration of CO₂ in ppmv,

146 and x are any boundary conditions which are Pliocene as opposed to PI, which can be any or none of
147 o = orography, v = vegetation and i = ice sheets). So, for example, Eov^{500} would be an experiment
148 using Pliocene orography and vegetation and with CO_2 at 500 ppmv, but with preindustrial ice sheets.
149

150 **2.2. Model description**

151 The model presented here is the Global Coupled (GC) 3.1 configuration of the UK's physical climate
152 model, HadGEM3-GC31-LL, which is the "CMIP6-class" UK Met Office physical climate model.
153 The *piControl* simulation for this model was conducted elsewhere as part of CMIP6, and is used here
154 for comparative purposes; see Williams *et al.* (2017), Kuhlbrodt *et al.* (2018) and Menary *et al.*
155 (2018) for further details on HadGEM3-GC31-LL and its *piControl* simulation. The *mPWP*
156 simulation presented here was run with identical components to those used in other CMIP6/PMIP4
157 simulations using this model, namely the *midHolocene* and *lig127k* simulations (Williams *et al.*
158 2020). The full title for this configuration is HadGEM3-GC31-LL N96ORCA1 UM10.7 NEMO3.6
159 (hereafter referred to as HadGEM3). The model was run using the Unified Model (UM), version
160 10.7, and included the following components: i) Global Atmosphere (GA) version 7.1, with an N96
161 atmospheric spatial resolution (approximately 1.875° longitude by 1.25° latitude) and 85 vertical
162 levels; ii) NEMO ocean version 3.6, including Global Ocean (GO) version 6.0 (ORCA1), with an
163 isotropic Mercator grid which, despite varying in both meridional and zonal directions, has an
164 approximate spatial resolution of 1° by 1° and 75 vertical levels; iii) Global Sea Ice (GSI) version 8.0
165 (GSI8.0); iv) Global Land (GL) version 7.0, comprising the Joint UK Land Environment Simulator
166 (JULES); and v) the OASIS3 MCT coupler. All of the above individual components are summarised
167 by Williams *et al.* (2017) and detailed individually by a suite of companion papers (see Walters *et al.*
168 2017 for GA7 and GL7, Storkey *et al.* 2017 for GO6 and Ridley *et al.* 2017 for GSI8). A summary of
169 the major changes in HadGEM3 and their impacts on the climate, relative to its most recent
170 predecessor (HadGEM2), are given in Williams *et al.* (2020). Here, the *mPWP* simulation was run on
171 NEXCS, which is a component of the Cray XC40 located at the UK Met Office. NEXCS is a
172 partition of the UK Met Office's platform, Monsoon, on which the *piControl* simulation was run,
173 thereby avoiding the potential caveat discussed in Williams *et al.* (2020) concerning different
174 computing platforms.

175

176 Details of the other models discussed here, namely previous generations of the same UK Hadley
177 Centre model and all of those included in PlioMIP2, are included in the Supplementary Material
178 (Section 1).

179

180 **2.3. Full Pliocene experiment design**

181 For the most part, the *mPWP* simulation presented here follows the protocol given in H16, discussed
182 below. The main difference is that we do not modify the land-sea mask (LSM), due to technical
183 challenges of modifying the ocean LSM and coupling it to the atmosphere in this model.

184

185 **2.3.1. Greenhouse gas atmospheric concentrations, aerosol emissions and ozone**

186 Following H16, atmospheric CO₂ concentration was modified in the *mPWP* simulation, from 280 to
187 400 ppmv. All other greenhouse gases, such as CH₄, N₂O and O₂, were kept as in the *piControl*
188 simulation. Likewise, aerosol emissions (e.g. organic- and black-carbon fossil fuels) and their
189 resulting oxidants were kept as in the *piControl* simulation, consistent with previous paleoclimate
190 simulations with this model (Williams *et al.* 2020).

191

192 Under strong surface warming, the thermal tropopause rises. In simulations with prescribed ozone
193 concentration it is important that the thermal tropopause remains below the ozone tropopause, in order
194 to avoid unphysical feedbacks associated with increasing cold point temperature (see, for example,
195 Hardiman *et al.* 2019). For this reason, ozone from the *IpctCO₂* simulation of the UK Earth System
196 Model (UKESM1, see Sellar *et al.* 2019), in which CO₂ concentrations are increased relative to 1850
197 levels at 1% per year, was prescribed here. UKESM1 uses the same physical climate configuration as
198 HadGEM3, but interactively simulates ozone chemistry. The ozone was taken from a 10-year period
199 of this UKESM1 simulation (years 51-60), during which the mean surface temperature was
200 approximately 2°C warmer than the *piControl* simulation. The value of 2°C was chosen as a
201 compromise between raising the ozone tropopause enough to avoid inconsistency with the thermal
202 tropopause, without introducing significant changes in ozone forcing relative to the *piControl*. The
203 impact of the ozone modification could be explored in future work, for example by using an ozone
204 profile from a UKESM1 simulation with a higher mean surface temperature (more consistent with the
205 HadGEM3 Pliocene warming, see Section 3), or by using the methodology outlined in Hardiman *et*
206 *al.* (2019), which was used for the CMIP6 Shared Socioeconomic Pathway (SSP) scenario simulations
207 with HadGEM3.

208

209 **2.3.2. Changes to boundary and initial conditions**

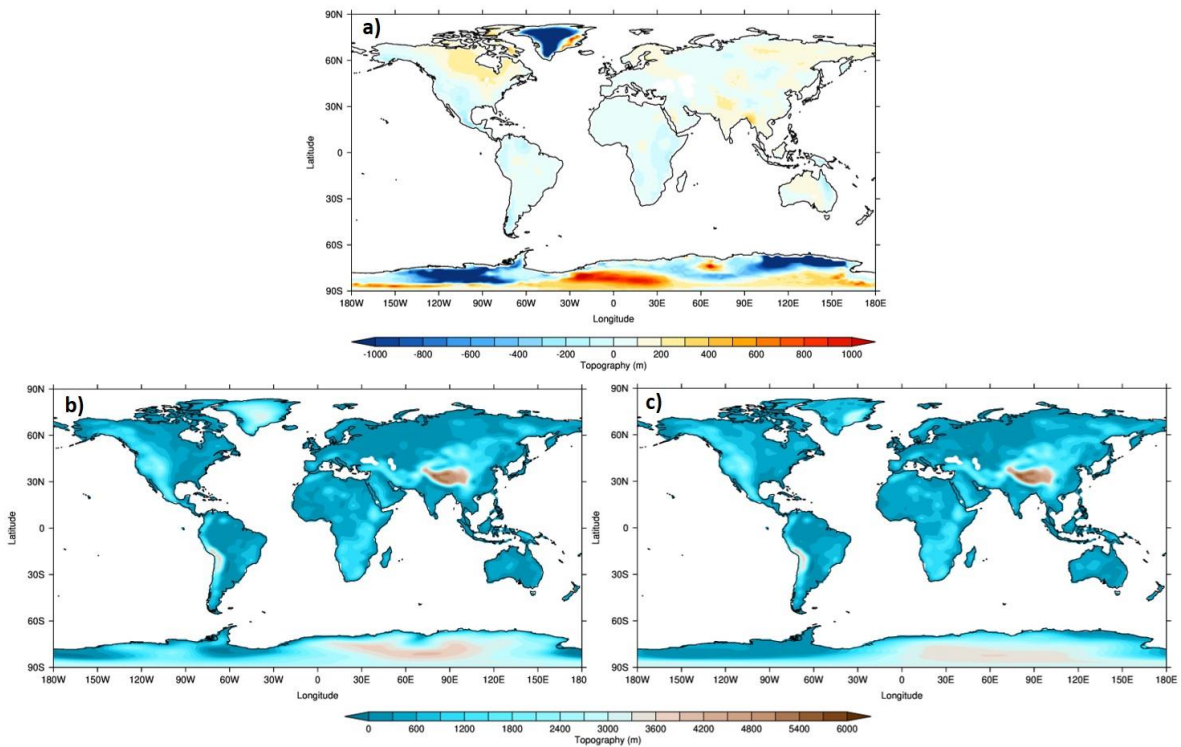
210 **2.3.2.1. Palaeogeography (including land-sea mask, orography and bathymetry)**

211 The *mPWP* simulation used an identical LSM to the *piControl* simulation which, if necessary, is
212 allowed under the experimental design laid out in H16. This differs from both the standard and
213 enhanced LSMs provided by H16 (accessible, with all other required boundary conditions, from the
214 US Geological Survey's PlioMIP2 website, http://geology.er.usgs.gov/egpsc/prism/7_pliomip2.html),
215 in that in both of these the gateways in the Bering Sea, the Canadian Archipelago and Hudson Bay are
216 closed, whereas in the HadGEM3 simulations only the Canadian Archipelago/Hudson Bay gateway is

217 closed; the Bering Strait is open (see Supplementary Material, Fig. S1). Likewise, the bathymetry
218 used here is also identical to the *piControl* simulation, for the same reasons.

219

220 The orography used in the *mPWP* simulation, however, does follow the protocol of H16. Here, an
221 anomaly is firstly created by subtracting the PRISM4 modern orography from the PRISM4 Pliocene
222 orography and then, after having been re-gridded to the model's own resolution, adding this to the
223 model's existing orography (see Section 2.3.2 in H16). The results are shown in Figure 1, where the
224 PRISM4 anomaly shows the largest changes are occurring over Greenland and Antarctica, with
225 smaller changes over the Himalayas, North America and Africa (Fig. 1a). When added to
226 HadGEM3's existing orography (Fig. 1b), the changes result most obviously in a lowering of
227 orography over Greenland, western and eastern Antarctica, and a raising of orography over central
228 Antarctica (Fig. 1c). Due to an early model instability relating to the steep orographic gradients in
229 western Antarctica, this region was smoothed in the final simulation (Fig. 1c).



230

231 Figure 1 - Changes to topography in HadGEM3 *mPWP* simulation. a) PRISM4 anomaly; b) Original field used in
232 HadGEM3 *piControl*; c) New field used in HadGEM3 *mPWP*, with smoothed topography over western Antarctica (final
233 version, used in simulation)

234

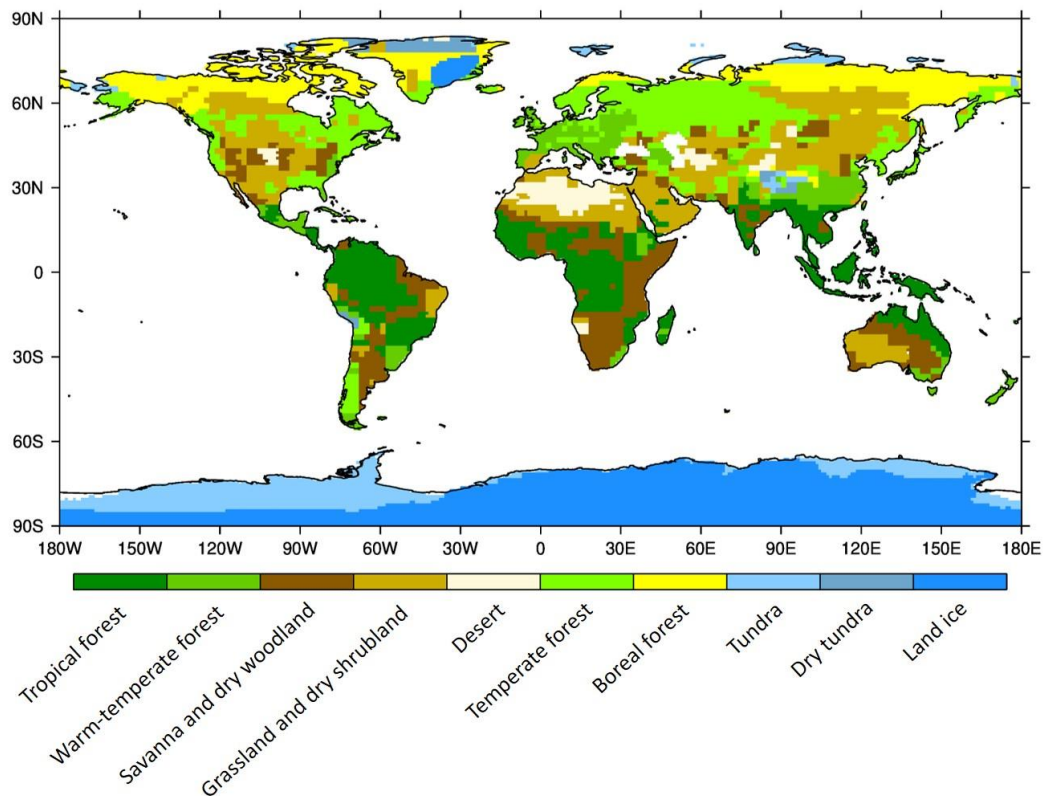
235 2.3.2.2. *Vegetation fractions (including urban, lakes and ice)*

236 As part of its GL configuration, both the *piControl* and *mPWP* simulations used the community land
237 surface model (JULES; see Best *et al.* 2011, Clark *et al.* 2011, Walters *et al.* 2019). In this land
238 surface model, sub-gridscale heterogeneity is represented by a tile approach (Essery *et al.* 2003), in

239 which each grid box over land is divided into five vegetated plant functional types (PFTs): broadleaf
240 trees (BLT), needle-leaved trees (NLT), temperate C3 grass, tropical C4 grass and shrubs. In addition
241 to these, there are four non-vegetated PFTs: urban areas, inland water (or lakes), bare soil and land
242 ice. This division of grid box into PFTs is consistent with both of the model's predecessors (see
243 Supplementary Material). With the exception of the urban tile, which was kept as PI to be consistent
244 with previous paleoclimate simulations with this model (Williams *et al.* 2020), all of these PFTs were
245 modified in the *mPWP* simulation.

246

247 The US Geological Survey's PRISM4 (Dowsett *et al.* 2016) vegetation reconstruction from Salzmann
248 *et al.* (2008) was used, provided as a megabiome reconstruction in PlioMIP2 (H16). This can be seen
249 in Figure 2, where there are ten listed megabiomes corresponding to those used in Harrison and
250 Prentice 2003: tropical forest, warm-temperate forest, savanna and dry woodland, grassland and dry
251 shrubland, desert, temperate forest, boreal forest, tundra, dry tundra and land ice.



252

253 Figure 2 - Ten megabiomes from PlioMIP2 used create the nine PFTs used in HadGEM3 *mPWP* simulation

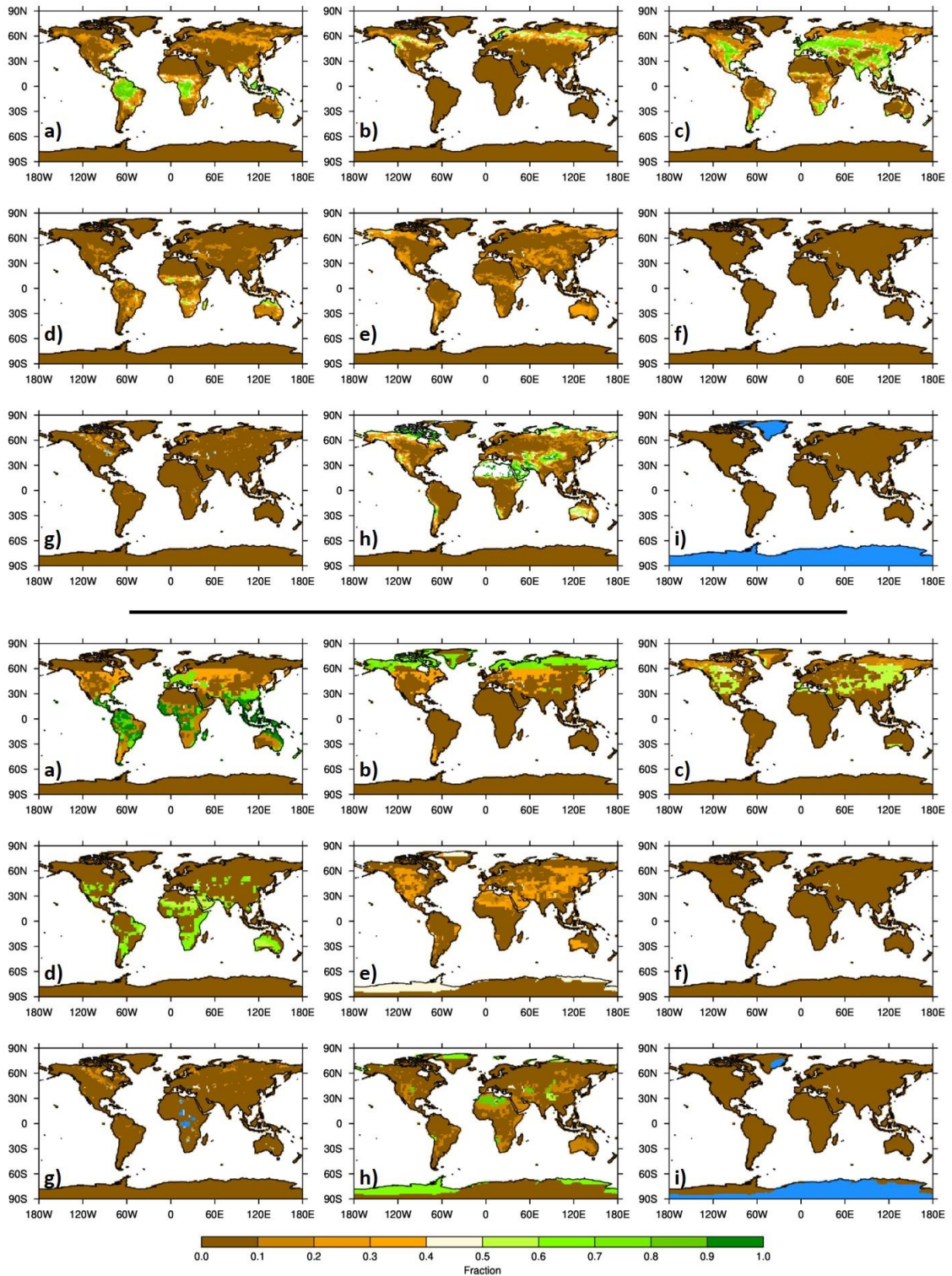
254

255

256

257

258 In order to translate the megabiomes from PRISM into the PFTs used by the model, a lookup table
259 was therefore required. Minimum and maximum bounds for each megabiome were firstly obtained,
260 based on values from Crucifix *et al.* 2005, and then estimates were made for each PFT within these
261 bounds by mapping the preindustrial megabiomes onto the preindustrial PFT in HadGEM3; the
262 resulting lookup table is shown in the Supplementary Material (Table S1). In this table, for example,
263 each land grid point with the megabiome “Tropical forest” is divided amongst the model PFTs as 92%
264 BLT, 5% bare soil, 2% tropical C4 grasses and 1% shrubs. The resulting 9 PFTs used in the *mPWP*
265 simulation, as well as those from the original *piControl*, are shown in Figure 3. The largest fractional
266 increases, relative to the *piControl*, occur for broadleaf trees and needleleaf trees (18% and 5%,
267 respectively; Fig. 3a and b) and the largest decreases occur for temperate C3 grass and land ice (15%
268 and 5%, respectively; Fig. 3c and i). In regions where there is no obvious match between the model’s
269 PFTs and the megabiomes, such as over western Antarctica (specified as tundra in the PRISM data), a
270 closest match was provided; in this case, a mix of bare soil and shrubs.



271

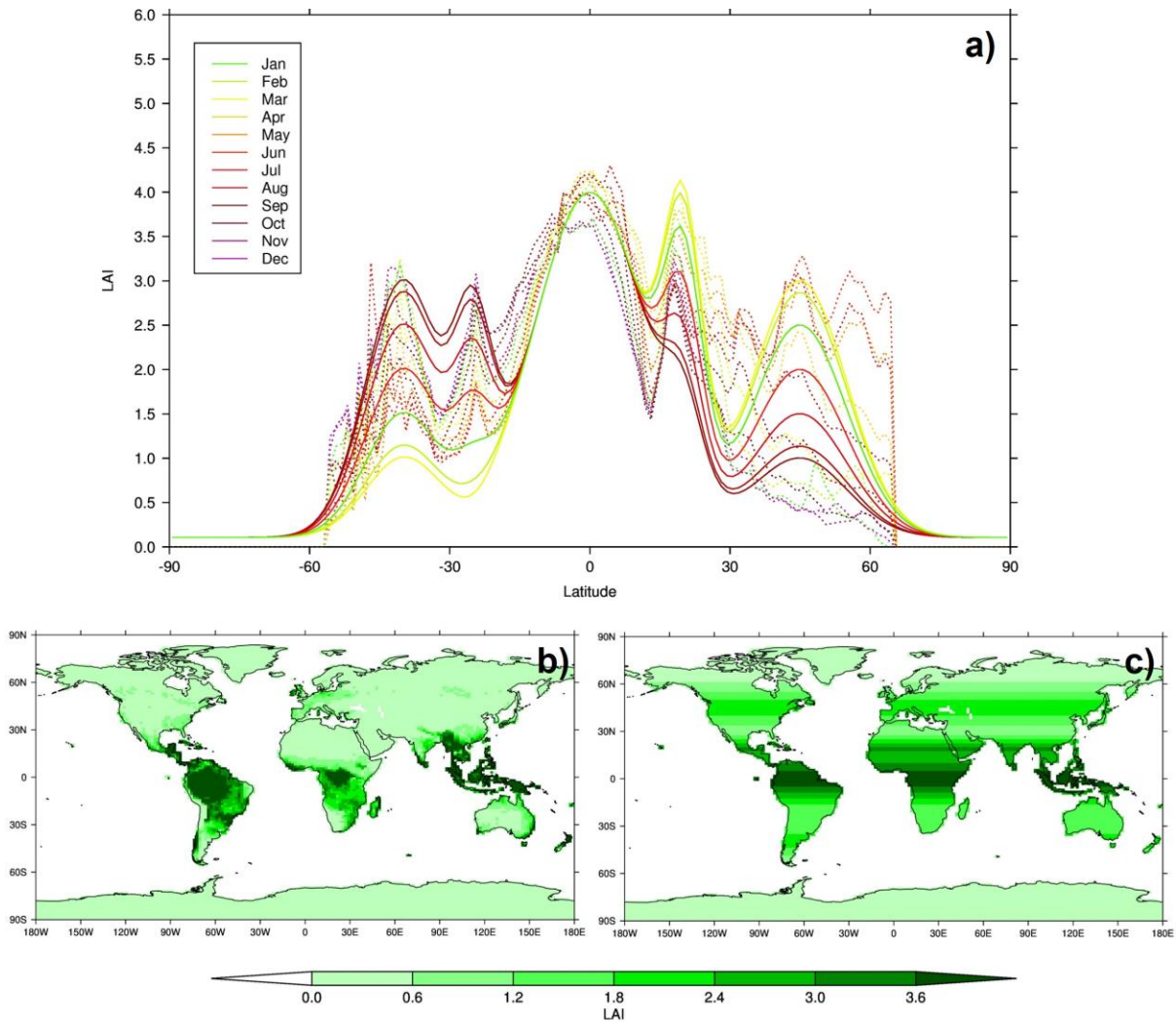
272 Figure 3 - Nine PFTs used in HadGEM3. Top half: *piControl* simulation, bottom half: *mPWP* simulation. Values in
 273 brackets show global mean differences (*mPWP* - *piControl*), expressed as a percentage. a) broadleaf trees (18%); b) needle-
 274 leaved trees (5%); c) temperate C3 grass (-15%); d) tropical C4 grass (6%); e) shrubs (3%); f) urban areas (no change); g)
 275 inland water (1%); h) bare soil (-12%); i) land ice (-5%)

276

277

278 2.3.2.3. *Vegetation functional types*

279 Alongside the vegetation fractions, both the *piControl* and *mPWP* simulations included two monthly-
280 varying vegetation functional types, namely leaf area index (LAI) and canopy height, both of which
281 are associated with each of the five vegetated PFTs. Given that no information was available from the
282 PRISM vegetation reconstruction concerning these fields, two methods were used to create Pliocene
283 LAI and canopy height. For LAI, a seasonally and latitudinally varying function was created from the
284 zonal means of the *piControl* (Figure 4), and used to build a new field for the Pliocene, for each
285 month and each PFT (see Fig. 4b and c for an example of the original *piControl* and the Pliocene
286 newly-created field, respectively, both showing LAI for BLT during January). This is because, in the
287 *piControl*, LAI varies both in time (i.e. seasonally) and space. Note that although LAI does go to zero
288 in the *piControl*, this was not allowed in the *mPWP* simulation because the Pliocene does have some
289 vegetation at high latitudes (see Figure 3); these functions were therefore increased by x (where $x =$
290 the mean of the ten grid points containing the lowest LAI), such that there is never zero LAI. In
291 contrast, canopy height in the *piControl* does not vary monthly, and has little variation spatially,
292 therefore canopy height in the *mPWP* simulation is set to the global mean of the *piControl* (see
293 Supplementary Material Fig. S2).



294

295 Figure 4 – LAI used in HadGEM3, for an example PFT (broadleaf trees). a) Function used to create LAI, where dashed
 296 lines show zonal mean from *piControl* simulation and solid lines show seasonally and latitudinally varying function used in
 297 the *mPWP* simulation; b) Example of functional types (broadleaf trees, January) used in *piControl* simulation; c) same as b)
 298 but for the *mPWP* simulation/
 299

300

300 2.3.2.3. Soil properties and snow depth

301 Under newly-created land ice based on the new Pliocene ice mask (i.e. in regions where there is no ice
 302 in the *piControl* but ice the *mPWP* simulation), soil parameters, soil dust properties and snow depth
 303 were set to be appropriate values for existing ice regions i.e. whatever these values are under ice in the
 304 *piControl* simulation are applied to the newly-created ice regions in the *mPWP* simulation.
 305

306

307 Conversely, and more importantly in this context (as the Pliocene represents an overall removal of
 308 ice), under newly-exposed land based on the new Pliocene ice mask (i.e. in regions where there is ice
 309 in the *piControl* but no ice in the *mPWP* simulation, primarily over Greenland and western
 310 Antarctica), the dominant vegetation fractions in these regions were firstly identified from the newly-
 310 created Pliocene vegetation. In this case, the dominant fractions were 40% shrubs and 60% bare soil.

311 Then, grid points containing this vegetation balance in the *piControl* were identified, and the soil
312 parameters, soil dust properties and snow depth values at these points were averaged. This average
313 value, for each of the above fields, was lastly inserted back into the *mPWP* simulation's newly-
314 exposed grid points; it is acknowledged that this introduces new dust emissions source regions, which
315 may well impact the resulting Pliocene climate state.

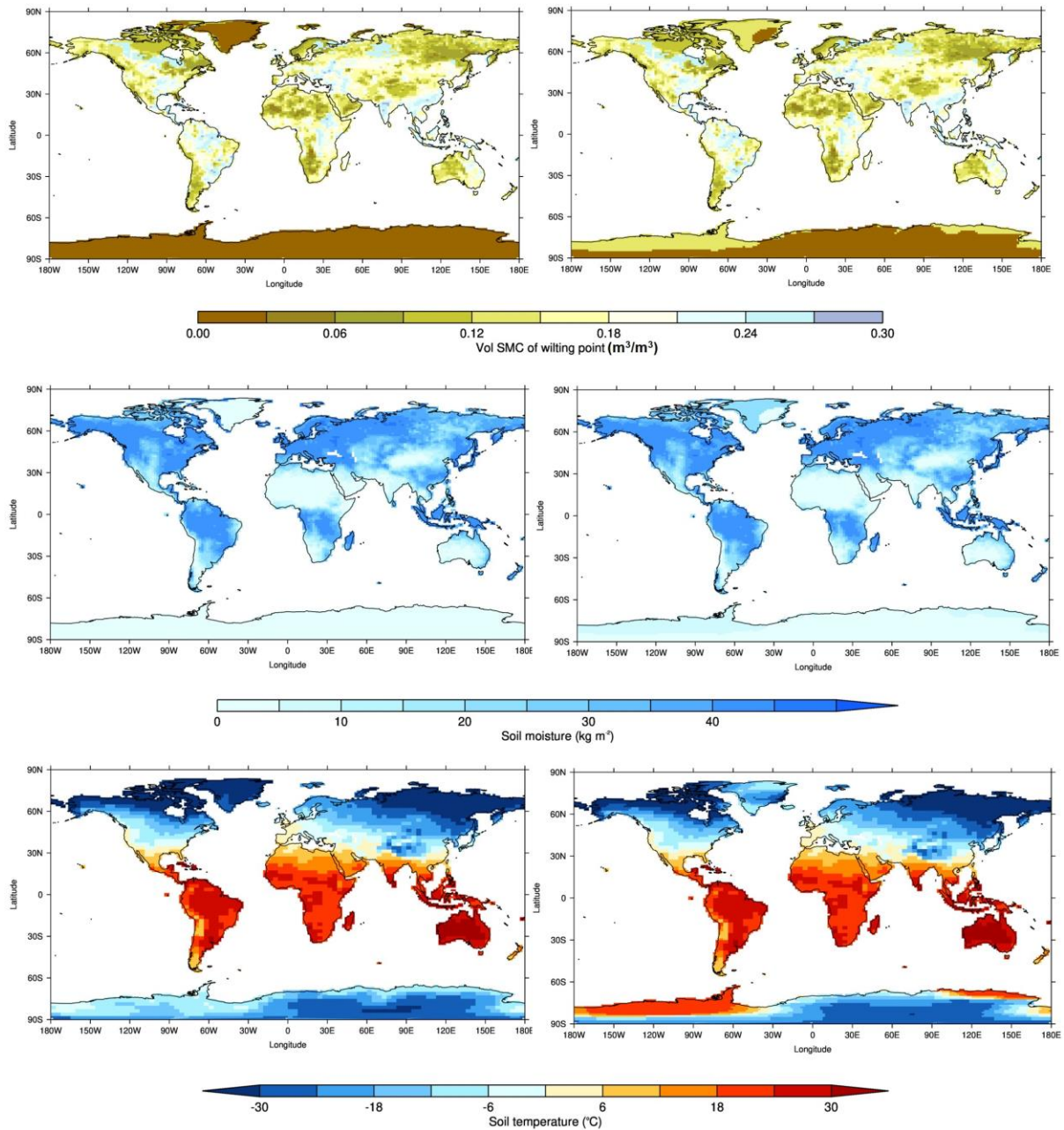
316

317 **2.3.2.4. Initial conditions**

318 Oceanic initial conditions, such as ocean temperature and salinity, were derived from the mean
319 equilibrium state of the *piControl* simulation. Some atmospheric initial conditions, such as those
320 relating to the land surface (e.g. soil moisture and soil temperature at four levels of depth), used the
321 same method as that applied to soil properties. These fields contain monthly varying values, therefore
322 appropriate timings were considered e.g. if the majority of grid points with the above balance were in
323 the Northern Hemisphere, then initial conditions during Northern Hemisphere summer were used for
324 newly-exposed regions in Greenland (and likewise during Southern Hemisphere summer for newly-
325 exposed regions in Antarctica). For the soil temperature field and particularly at upper levels, this
326 process resulted in sharp temperature gradients across western Antarctica, therefore the field was
327 spatially smoothed so that the gradients were more consistent with those in the *piControl*. Examples
328 of the above soil-related fields are shown in Figure 5 for an example month and vertical level. A
329 complete list of the soil parameters and soil dust properties, and how each were changed relative to
330 the *piControl*, are shown in the Supplementary Material (Fig. S3 and Fig. S4, respectively).

331

332 Outside of the ice regions (i.e. outside Greenland and Antarctica), in the *mPWP* simulation the above
333 soil-related fields were kept identical as in the *piControl*.



334

335 Figure 5 – Example of soil-related fields used in HadGEM3. Left-hand column: *piControl* simulation, right-hand column:
 336 *mPWP* simulation. First row: Soil parameters (example shows Volumetric soil moisture content at wilting point); Second
 337 row: Soil moisture (example shows January, top-level); Third row: Soil temperature (example shows January, top-level).
 338 Complete list of fields shown in Supplementary Material Fig. S3 and S4

339

340 2.3.3. Changes to input parameters

341 A small number of model input parameters were changed in the *mPWP* simulation, to make the model
 342 more stable under the Pliocene boundary conditions. Firstly a parameter governing the implicit solver
 343 for unstable atmospheric boundary layers was increased, and secondly three parameters for the
 344 treatment of canopy snow were made consistent between BLT and NLT. The same parameter
 345 changes will be included in the subsequent version of the physical model (GC4), in order to address
 346 occasional model failures which were seen following the release of GC3.1. They will be described in

347 more detail in a GC4 model documentation paper, however testing of those changes for GC4 has
348 found that they have no detectable impact on model climatology.

349

350 **2.4. Modified *piControl* simulation**

351 Given that the official CMIP6 *piControl* simulation did not use the aforementioned model input
352 parameter changes, a slightly modified version of this simulation was re-run (simulation ID: u-bq637),
353 identical to the *piControl* other than including the parameter changes outlined in Section 2.3.3
354 (hereafter referred to as the *piControl_mod* simulation). This was run for 200 years, and the last 50-
355 year climatology is considered here in Sections 3 and 4.

356

357 **3. LARGE-SCALE FEATURES OF HADGEM3**

358 **3.1. Spin-up phase**

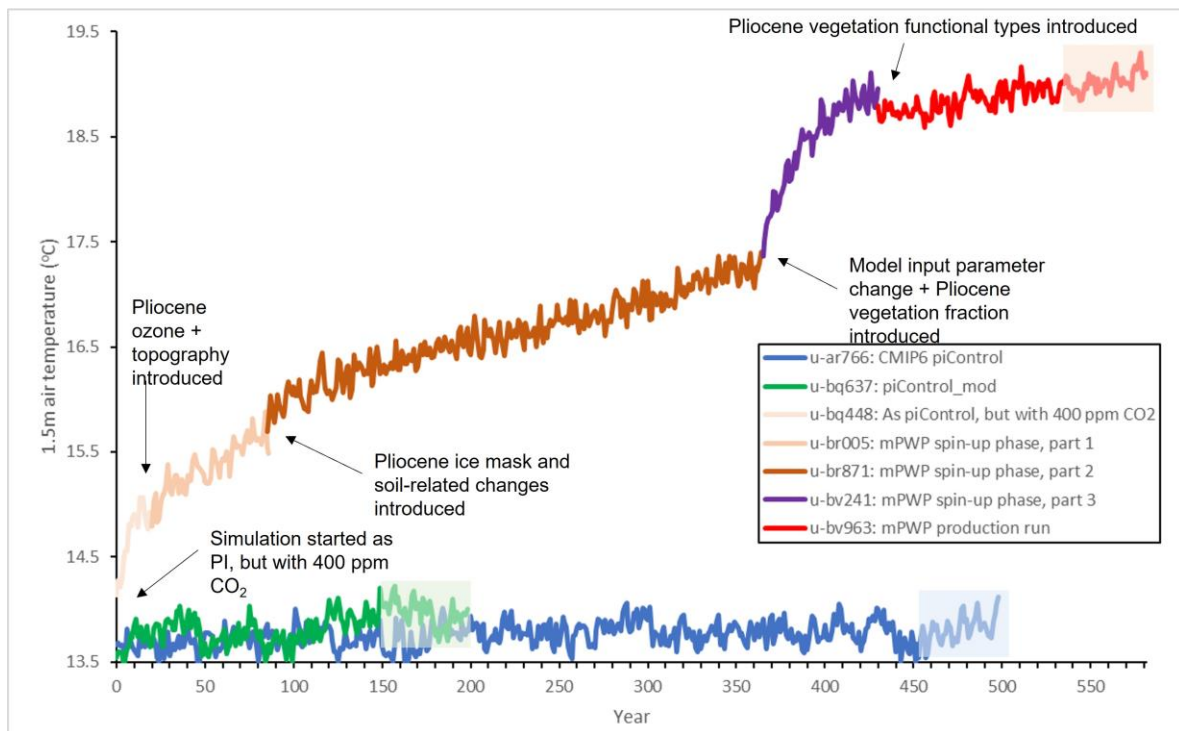
359 Consistent with other paleoclimate model experiments, the simulation should be run for as long as
360 possible to allow the model to reach a state of equilibrium, before the climatology is calculated over
361 the last 30, 50 or 100 years (Lunt *et al.* 2017). With this model, however, running for thousands of
362 years (especially important in obtaining oceanic equilibrium) was unfeasible given time and resource
363 constraints. By the end of the simulation, therefore, there was a total of 576 years for the *mPWP*
364 simulation, 526 of which are considered spin-up and 50 of which form the final climatologies; this is
365 approximately consistent with the 652 years of spin-up used by Menary *et al.* (2018).

366

367 **3.1.1. Evolution of *mPWP* simulation**

368 The HadGEM3 *mPWP* simulation was run in multiple parts, each starting from the endpoint of the
369 last, and each introducing additional boundary conditions so as to gradually move from PI conditions
370 to full Pliocene conditions. The *mPWP* simulation was started from the endpoint of the CMIP6
371 *piControl* simulation, specifically the last part of its spin-up phase (u-aq853), consistent with other
372 CMIP6 HadGEM3 paleoclimate simulations such as those of the mid-Holocene and Last Interglacial
373 periods (see Williams *et al.* 2020). The evolution of the *mPWP* simulation is shown in Figure 6,
374 where each stage is labelled and the resulting impact on the global mean 1.5 m air temperature is
375 shown. The first part of the *mPWP* simulation (u-bq448) is a straight copy of the CMIP6 *piControl*
376 production run (u-ar766), with no modifications other than increasing the atmospheric CO₂ to 400
377 ppmv; identical, therefore, to an E⁴⁰⁰ experiment following the naming convention of H16. This ran
378 for ~20 model years, before branching off to a new suite (u-br005) and introducing atmospheric ozone
379 appropriate for Pliocene conditions and Pliocene orography (see Section 2.3.1 and 2.3.2,
380 respectively). This ran for ~60 model years, before branching off to a new suite (u-br871) and
381 introducing a Pliocene-appropriate ice mask along with appropriate values for soil parameters, soil
382 dust, soil moisture, soil temperatures and snow depth over these newly created ice regions (see
383 Section 2.3.2); this, therefore would be the Eoi⁴⁰⁰ experiment following the naming convention of

384 H16. It should be noted, however, that at this stage this naming convention is not strictly consistent
 385 with that used by H16, because they specify that orography, lakes and soils should be modified in
 386 unison, and therefore *o* signifies changes to orography, bathymetry, land-sea mask, lakes and soils
 387 together. In contrast, at this stage of the simulation, most boundary conditions are consistent with the
 388 experimental design of H16, except vegetation, soils in non-ice regions and lakes. This ran for ~280
 389 model years (during which time the task of creating appropriate Pliocene vegetation was completed),
 390 before branching off to a new suite (u-bv241) and introducing a minor parameter change to allow
 391 inclusion of the Pliocene vegetation (see Section 2.3.3), as well as the full Pliocene vegetation
 392 fractions. This ran for a further ~60 years, to check the stability of the model in response to the
 393 vegetation change, before branching off to a new and final suite (u-bv963), in which the full Pliocene
 394 vegetation functional types were introduced. This ran for ~150 years, with the final climatology
 395 (presented here in Section 3 and 4) being taken from the last 50 years i.e. allowing a 100-year buffer
 396 between the final update to the model and the actual results.



397
 398 Figure 6 – Annual global mean 1.5 m air temperature from the HadGEM3 *mPWP* spin-up phase and production run, as well
 399 as the CMIP6 *piControl* and the *piControl_mod*. Labels show introduction of each new Pliocene element. Climatologies
 400 discussed here are taken from final 50 years of each simulation (shown by shaded boxes). See Williams *et al.* (2020) for the
 401 *piControl* spin-up phase that preceded these simulations.

402
 403 As well as the various stages of the *mPWP* simulation, Figure 6 also shows timeseries from the
 404 official ~500 year CMIP6 *piControl* simulation (Kuhlbrodt *et al.* 2018 and Menary *et al.* 2018) and
 405 the 200 year *piControl_mod* conducted here, and Figure S7 shows climatologies of 1.5 m temperature
 406 and surface precipitation calculated over the last 50 years of each simulation. As the figures show,
 407 there is little or no difference between the two PI simulations (also suggested above in Section 2.3.3);

408 using temperature as an example, over the last 50 years of the simulations there is a mean of 13.79°C
 409 and 13.97°C for the *piControl* and *piControl_mod* respectively, and a standard deviation of 0.13°C for
 410 both, further confirming the negligible impact of the model parameter change in the model
 411 climatology.

412

413 **3.1.2. Atmospheric and oceanic equilibrium of the *mPWP* simulation**

414 Concerning atmospheric equilibrium, Table 1 shows summary statistics for annual global mean 1.5 m
 415 air temperature and net top of atmosphere (TOA) radiation from the last 50 years of the *mPWP*
 416 simulation, compared to both the *piControl* and *piControl_mod* simulations; see Figure 6 for the
 417 entire timeseries of Pliocene 1.5 m air temperature, and Figure S5 in the Supplementary Material for
 418 the TOA radiation equivalent.

Variable	<i>piControl</i>	<i>piControl_mod</i>	<i>mPWP</i>
1.5m air temperature trends (°C century⁻¹)	0.51	-0.47	0.34
TOA radiation trends (W m⁻² century⁻¹)	0.02	-0.2	-0.17
Mean TOA radiation (W m⁻²)	0.18	0.21	0.88
Global ocean volume-mean temperature trends (°C century⁻¹)	0.03	0.04	0.21
Global ocean volume-mean salinity trends (psu century⁻¹)	0.0004	-0.0002	-0.004

419

420 Table 1 - Centennial trends (calculated via a linear regression) and climatology over the last 50 years of the simulations. A
 421 positive TOA imbalance indicates a net loss of energy from the Earth System

422

423 Although the *mPWP* simulation is clearly warming considerably during the ~500 year run (and
 424 especially when the Pliocene vegetation fraction is introduced), with trends of 0.77°C century⁻¹, it
 425 levels off over the final 50 years, with trends of 0.34°C century⁻¹ (Table 1). These values are higher
 426 than those considered by some (e.g. Menary *et al.* 2018) to be acceptable for equilibrium, however
 427 given time and resource constraints it was not possible to run the simulation further. The spatial
 428 patterns of these trends, shown in Figure S6 in the Supplementary Material, shows the majority of the
 429 warming occurring over high latitude regions in both Hemispheres, related to the removal of the ice
 430 sheets and sea ice loss. By the end of the *mPWP* simulation, the mean TOA radiation balance is 0.88
 431 W m⁻², significantly higher than either of the PI simulations suggesting that the *mPWP* simulation is
 432 not yet in full atmospheric equilibrium. This TOA imbalance is reducing at a rate of 0.17 W m⁻²

433 century⁻¹ at the end of the simulation. A brief discussion of how the HadGEM3 *mPWP* simulation's
434 atmospheric equilibrium compares to that of the other Hadley Centre models presented here
435 (introduced in Section 4) is given in the Supplementary Material (see Section 2 and Table S2).

436

437 When the *mPWP* simulation was stopped, the global annual mean 1.5 m temperature was
438 approximately 19°C (Fig. 6). A Gregory plot (Gregory *et al.* 2004) of the evolution of TOA energy
439 imbalance and surface temperature can indicate how much more warming the model may have
440 experienced if it had been run to full equilibrium. The results of this analysis suggest the model
441 would come to equilibrium ~1.5°C higher (see Supplementary Material, Fig. S8), at 20.5°C i.e. an
442 anomaly relative to preindustrial of 6.6°C. This is the case when the extrapolation is carried out on
443 either of the final two parts of the simulation (in red and in purple in Fig. S8), suggesting that the
444 introduction of the Pliocene vegetation functional types is not having a great impact on the final
445 global mean temperature. However, this analysis is associated with some uncertainty, related to the
446 interannual variability in temperature and TOA energy imbalance, and to the fact that the linear
447 extrapolation may not be appropriate if the feedbacks vary non-linearly (e.g. Knutti *et al.* 2015).

448

449 As an example of oceanic equilibrium, Table 1 also shows summary statistics for volume integral
450 annual global mean ocean temperature and salinity from the end of the *mPWP* simulation, compared
451 to both the *piControl* and *piControl_mod* simulations; see Figure S9 in the Supplementary Material
452 for the Pliocene timeseries. Ocean temperature is steadily increasing throughout the *mPWP*
453 simulation, and likewise ocean salinity is steadily decreasing (Fig. S9). Freshwater fluxes to the
454 ocean representing iceberg calving and ice sheet basal melt are calibrated for the *piControl*, as
455 described in Sellar *et al.* (2020). These fluxes are calibrated to match the ice sheet surface mass
456 balance (SMB) expected in the *piControl*, so that salinity drift is minimised. The Pliocene SMB is
457 smaller than that in the *piControl*, and hence net flux of water to the ocean is positive, leading to the
458 salinity drift. If compute resources allowed for a much longer Pliocene simulation, this ocean flux
459 could be calibrated to Pliocene SMB once the temperature and SMB had stabilised, or calculated
460 iteratively. The long-term trends, Table 1, provide similar conclusions to those from the atmospheric
461 trends, with for example centennial temperature trends of 0.21°C century⁻¹ being much higher than the
462 PI simulations (0.03°C century⁻¹ and 0.04°C century⁻¹ for the *piControl* and *piControl_mod*,
463 respectively). Although these values again do not meet the criteria of Menary *et al.* (2018) for
464 oceanic equilibrium, given the aforementioned computational cost of this model it was not possible to
465 run the simulations further; this is even more true in the ocean, which would require many thousands
466 of years of model simulation to reach equilibrium. This compromise has been equally necessary for
467 other computationally expensive paleoclimate simulations (e.g. Williams *et al.* 2020).

468

469 **3.2. Simulation comparison: *mPWP* versus *piControl_mod* climatologies**

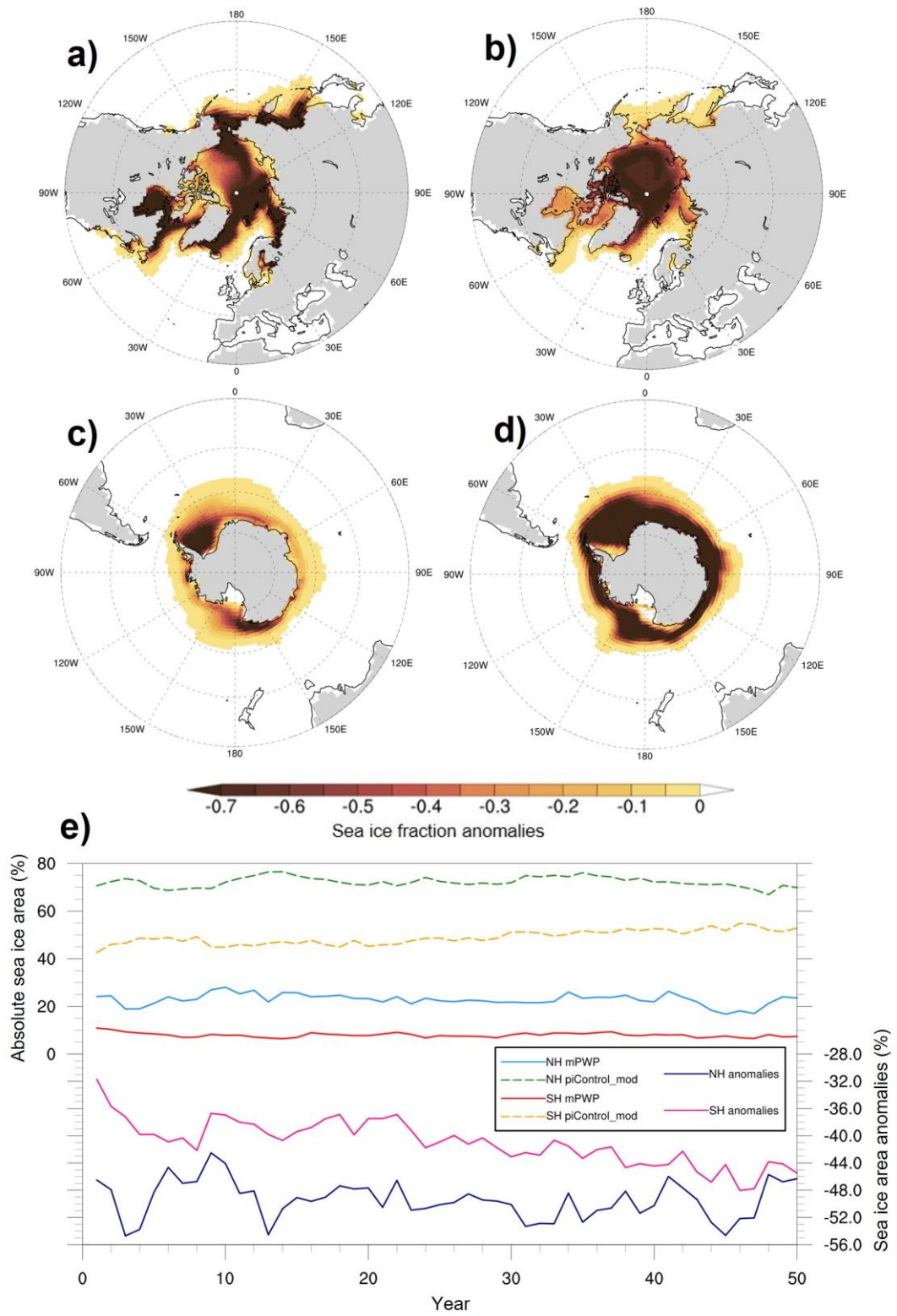
470 Here the focus is on mean differences between the HadGEM3 *mPWP* simulation and its
471 corresponding modified PI simulation, *piControl_mod* (Section 2.4). All of the following discussion
472 and figures relate to climatologies calculated over the last 50 years of the simulations, and all are
473 anomalies i.e. Pliocene - PI. Annual and seasonal mean summer/winter 1.5 m air temperature
474 (hereafter referred to as near-surface air temperature, SAT) anomalies are shown in Figure 7. The
475 annual global mean SAT anomaly for this 50-year climatology is 5.1°C. Warming relative to the PI is
476 evident throughout the year and globally, but more so over: i) landmasses (6.8°C and 4.5°C for the
477 annual mean SAT over land and ocean, respectively); ii) the Northern Hemisphere (8.5°C and 6.3°C
478 for annual mean SAT in the Northern and Southern Hemisphere extratropics (>45°), respectively).
479 Warming is also evident over high latitudes (>60°) of both hemispheres (10.9°C and 8.5°C for the
480 Northern and Southern Hemisphere, respectively, and exceeding 12°C in some places). These
481 particular metrics were chosen to be consistent with those used by H20 (see Section 4.2). Over the
482 tropics (20°N-20°S) the amount of warming is less than at higher latitudes, but the Pliocene is still
483 much warmer than the PI with annual mean SAT anomalies of 4.6°C and 3.7°C when averaged over
484 tropical land and ocean, respectively. This global and regional warming is consistent with, albeit
485 slightly warmer than, other work, namely the results from PlioMIP1 (Haywood *et al.* 2013) and
486 PlioMIP2 (see Section 4.2). The majority of the annual mean warming (Fig. 7a) in Northern
487 Hemisphere high latitudes is accounted for during that hemisphere's winter (December-February,
488 DJF) with a mean warming of 15°C (Fig. 7b), and likewise the majority of the annual mean warming
489 in Southern Hemisphere high latitudes is accounted for during that hemisphere's winter (June-August,
490 JJA) with a mean warming of 10.6°C (Fig. 7c). If the entire hemisphere, rather than >60°, is
491 considered, then this greater winter contribution to the annual mean is still true, although less so (e.g.
492 5.6°C, 6.1°C and 5.4°C for the annual, DJF and JJA means respectively in the Northern Hemisphere).
493

494 The regions of polar SAT increases, and seasonal variation, are likely explained by the changes in sea
495 ice, shown in Figure 8 (for the absolute values in sea ice fraction, see Fig. S10 in the Supplementary
496 Material). Reductions in sea ice are shown throughout the year in both hemispheres, consistent with
497 previous work (e.g. Cronin *et al.* 1993, Howell *et al.* 2016, Moran *et al.* 2006, Polyak *et al.* 2010).
498 Here, although a reduction in sea ice (of up to 70%) is evident throughout the year in either
499 hemisphere, at the seasonal timescale the largest loss (exceeding 70% in some places, such as the
500 polar Arctic and Antarctic) is seen during each hemisphere's winter (Fig. 8a and 8d). The
501 regions/timings of maximum warming (Fig. 7b-c) correspond well to the regions/timings of maximum
502 sea ice loss, implying a role for the sea ice-albedo feedback. When sea ice area is averaged over each
503 hemisphere (Fig. 8e), the Northern Hemisphere is clearly losing more sea ice in the *mPWP* simulation
504 (relative to the *piControl_mod*) than the Southern Hemisphere. However the amount of loss in the
505 Southern Hemisphere is steadily increasing during the last 50 years of the *mPWP* simulation,

506 suggesting that had the model been allowed to run to full equilibrium, the difference between the
 507 hemispheres would be reduced.

508

509 Figure 7 – 1.5 m air temperature climatology differences ($mPWP - piControl_mod$) from HadGEM3. a) Annual; b) DJF; c)
 510 JJA

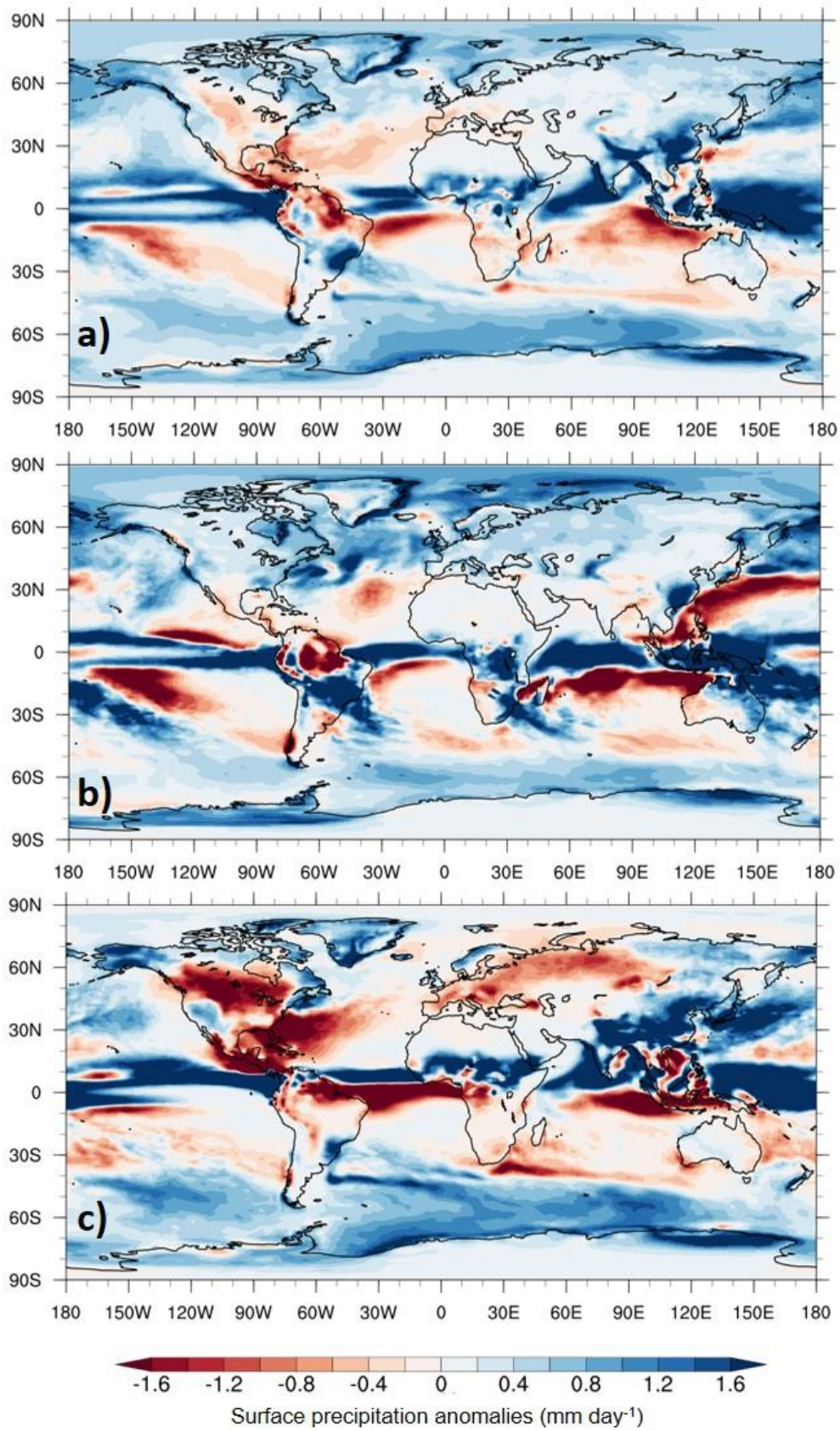


511

512 Figure 8 – Sea ice fraction climatology differences ($mPWP - piControl_mod$) from HadGEM3: a) Northern Hemisphere
513 DJF, b) Northern Hemisphere JJA, c) Southern Hemisphere DJF, d) Southern Hemisphere JJA, e) Mean sea ice area (both
514 absolute values and differences) averaged over either hemisphere

515

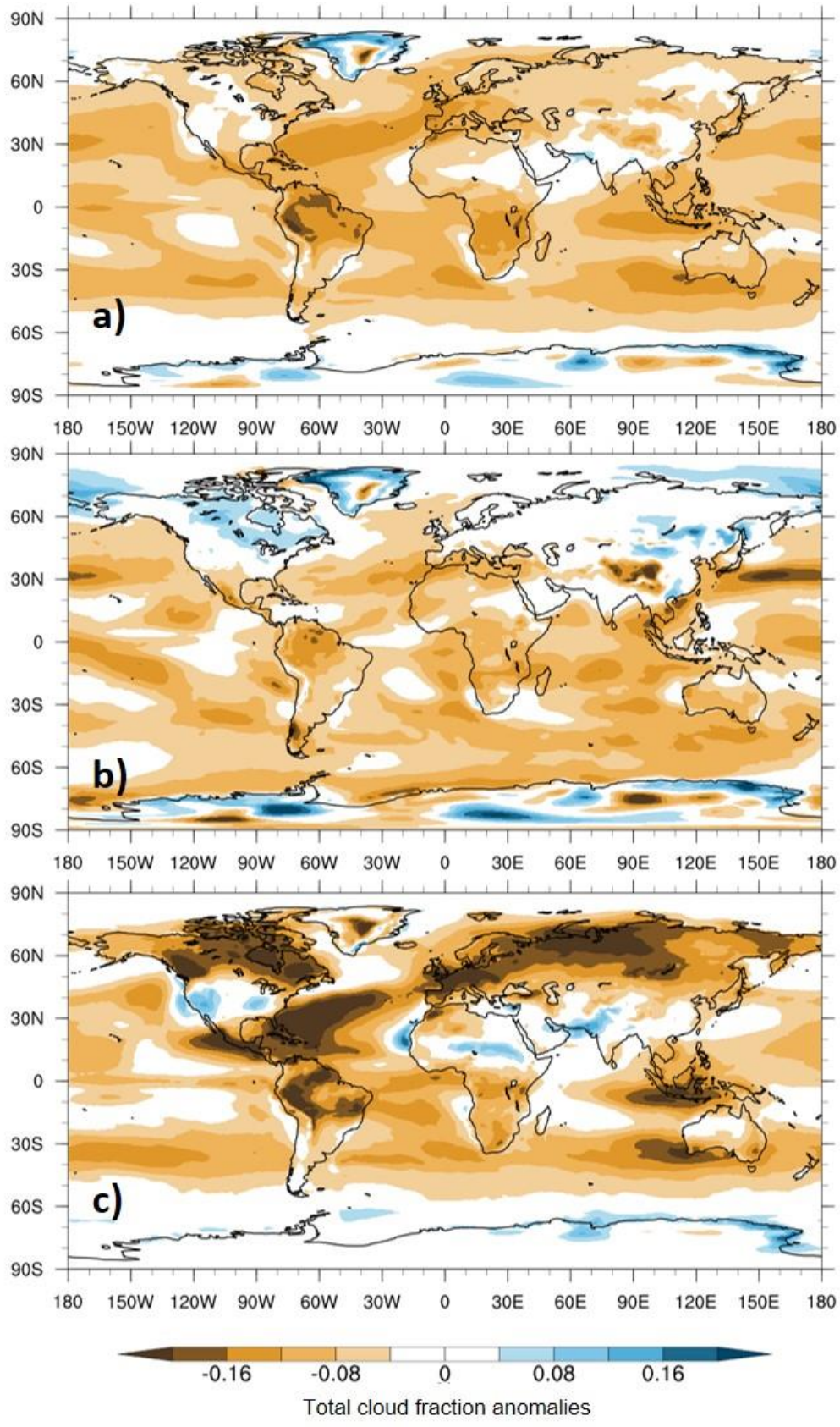
516 Annual and seasonal mean surface daily precipitation anomalies are shown in Figure 9. The annual
517 global mean precipitation anomaly for this 50-year climatology is 0.34 mm day^{-1} . In addition to the
518 precipitation increases at high latitudes at the annual timescale (Fig. 9a), which are again mostly
519 accounted for by changes during the Northern and Southern Hemisphere's winter (Fig. 9b and c,
520 respectively), the largest change relative to the PI is a northward displacement of the ITCZ. All
521 timescales are showing wetter conditions over oceans to the North of the equator and drier conditions
522 over oceans to the South of the equator. This is similar to work by Li *et al.* (2018), who suggested a
523 poleward movement of Northern Hemisphere monsoon precipitation in PlioMIP1. There is also a
524 noticeable enhancement of monsoon systems such as the East Asian and West African monsoon,
525 consistent with previous work (e.g. Zhang *et al.* 2013, 2016). In some places, these changes exceed
526 $\sim 2 \text{ mm day}^{-1}$, geographically consistent with (albeit again much higher than) other work, such as the
527 multi-model ensemble mean (MME) from PlioMIP2 models where increases rarely exceed $\sim 1.2 \text{ mm}$
528 day^{-1} (see Section 4.2). These changes, and indeed the temperature changes over Northern
529 Hemisphere landmasses, may be associated with changes to the total cloud cover, shown in Figure 10.
530 Although the changes are small at the annual timescale (Fig. 10a), during Northern Hemisphere
531 winter (Fig. 10b) there is a noticeable increase in cloud cover (of $\sim 10\%$) over high latitude regions,
532 corresponding to the increases in precipitation. Likewise, during Northern Hemisphere summer (Fig.
533 10c) there is a large reduction (over 20% in places) in cloud cover, especially over Northern
534 Hemisphere landmasses; these regions, such as Europe and Northern Asia, correspond well to the
535 areas of decreased precipitation and increased temperature.



536

537 Figure 9 – Surface precipitation climatology differences ($mPWP - piControl_mod$) from HadGEM3. a) Annual; b) DJF; c)

538 JJA



539
 540 Figure 10 – Total cloud fraction climatology differences ($mPWP - piControl_mod$) from HadGEM3. a) Annual; b) DJF; c)
 541 JJA
 542

543 **4. COMPARISON OF HADGEM3 WITH OTHER MODELS AND PROXY DATA**

544 **4.1. Model-model and model-data comparison: Different generations of UK model versus proxy**
 545 **data**

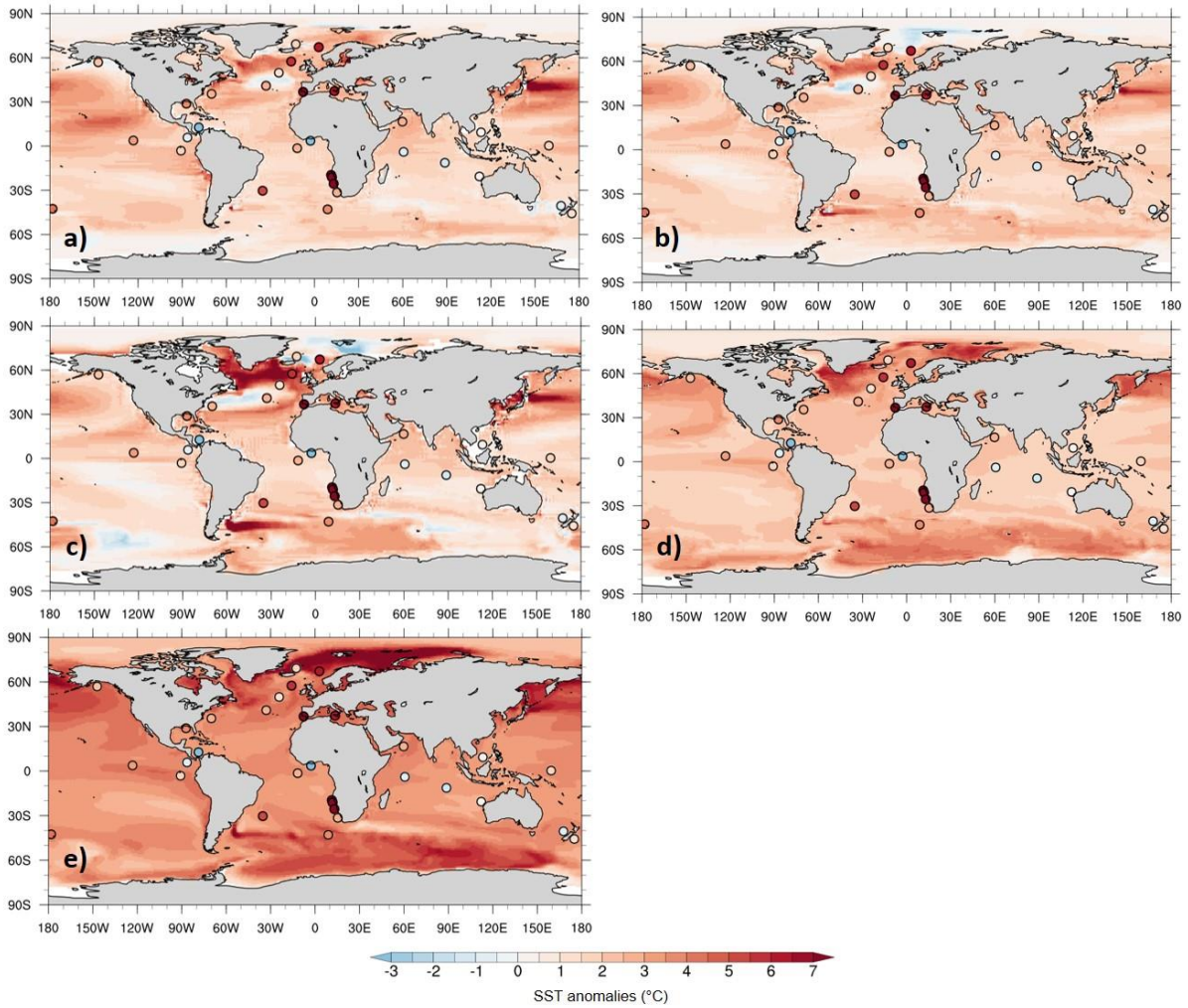
546 Here the focus is on mean SST differences between different generations of the UK’s physical climate
 547 model, starting with three Pliocene simulations using the original fully-coupled climate model
 548 HadCM3, then a simulation from the more recent HadGEM2 and finally the *mPWP* simulation from
 549 HadGEM3. See Supplementary Material for details of these older models. For HadCM3, three
 550 separate Pliocene simulations (and corresponding PIs) are used; the first two were conducted by Lunt
 551 *et al.* (2011) and Bragg *et al.* (2012), and are referred to as HadCM3-PRISM2 and HadCM3-
 552 PlioMIP1, respectively (see Table 2). This is to distinguish them from a third version of the same
 553 model included in PlioMIP2, referred to here as HadCM3-PlioMIP2.

Model	Model name here	MIP	Boundary conditions	Reference
HadCM3	HadCM3-PRISM2	-	PRISM2	Lunt <i>et al.</i> 2011
HadCM3	HadCM3-PlioMIP1	PlioMIP1	PRISM3	Bragg <i>et al.</i> 2012
HadCM3	HadCM3-PlioMIP2	PlioMIP2	PRISM4	Hunter <i>et al.</i> 2019
HadGEM2-AO	HadGEM2	PlioMIP1	PRISM3	Tindall and Haywood 2020
HadGEM3-GC31-LL	HadGEM3	PlioMIP2	PRISM4	Presented here

554
 555 Table 2 - Different generations of the UK physical climate model used here, and their involvement with PlioMIP
 556

557 Multi-proxy SST data from the KM5c interglacial, compiled by McClymont *et al.* (2020), were used
 558 for comparative purposes. Here, they focus on a narrow time-slice from 3.195 to 3.215 Ma, and
 559 compile the SST data from two proxies: an alkenone-derived $U^{K'}_{37}$ index (Prahl and Wakeham, 1987)
 560 and foraminifera calcite Mg/Ca (Delaney *et al.* 1985), with the resulting data comprising the PlioVAR
 561 synthesis and covering 32 locations between 46°S-69°N (McClymont *et al.* 2020).

562
 563 Maps of annual mean SST anomalies from the simulations, overlaid with the proxy data, are shown in
 564 Figure 11 and summary statistics are shown in Table 3.



565
 566 Figure 11 – Annual mean SST differences (Pliocene – PI) from different generations of the UK’s physical climate model. a)
 567 HadCM3-PRISM2; b) HadCM3-PlioMIP1; c) HadCM3-PlioMIP2; d) HadGEM2; e) HadGEM3. Background gridded data
 568 shows model simulations, filled circles show SST proxy data from McClymont *et al.* (2020)
 569
 570

	HadCM3-PRISM2	HadCM3-PlioMIP1	HadCM3-PlioMIP2	HadGEM2	HadGEM3
Global mean (°C)	1.63	1.53	1.67	2.29	3.80
RMSE	3.55	3.62	3.59	3.23	3.36

571
 572 Table 3 - Global annual mean SST anomalies from Pliocene simulations using different generations of the UK’s physical
 573 climate model, and RMSE values between simulations and SST proxy data from McClymont *et al.* (2020)
 574
 575
 576

577 The global annual SST anomaly for HadGEM3 is 3.8°C, followed by HadGEM2 at 2.3°C, and then
578 1.7°C, 1.5°C and 1.6°C for the three HadCM3 simulations (starting with the most recent, HadCM3-
579 PlioMIP2; see Table 3). Comparing the newest model (HadGEM3) with the oldest model (HadCM3-
580 PRISM2), which have an anomaly of 3.8°C and 1.6°C respectively, clearly the most recent generation
581 is showing a much warmer Pliocene.

582

583 Comparing an earlier generation of the model with a later generation, but with identical boundary
584 conditions (HadCM3-PlioMIP1 and HadGEM2, respectively; Fig. 11b and Fig. 11d), aside from the
585 greater overall warming (2.3°C in HadGEM2 versus 1.5°C in HadCM3-PlioMIP1) already discussed
586 above, the main spatial patterns of warming are similar, with both showing the greatest warming over
587 the Labrador Sea and the north-west Pacific and HadGEM2 showing greater polar amplification
588 overall. In part thanks to this high latitude warming, root mean squared error (RMSE) values are
589 3.2°C and 3.6°C for HadGEM2 and HadCM3-PlioMIP1, respectively, showing a greater agreement
590 between the proxy data and HadGEM2 (Table 3).

591

592 Likewise, comparing the other older model with the most recent (HadCM3-PlioMIP2 and HadGEM3,
593 respectively; Fig. 11c and Fig. 11e), the spatial patterns of warming differ more widely, with
594 HadGEM3 showing widespread Northern Hemisphere high latitude warming that is not shown by
595 HadCM3-PlioMIP2 at all, other than in the Labrador Sea. HadGEM3, and indeed HadGEM2, are
596 displaying a greater extent of polar amplification in both hemispheres (Fig. 11d-e). As the warmest
597 model, HadGEM3 (RMSE = 3.4°C) is showing less agreement with the proxy data than HadGEM2
598 (RMSE = 3.2°C), likely because it is so warm that the discrepancy with the colder proxy data
599 locations (such as in the Indian Ocean, near New Zealand or off equatorial Africa) is greater (Fig.
600 11e). This is in spite of the fact that, in the warmer proxy data locations (such as in the North Atlantic
601 and Arctic) HadGEM3 is closer to the proxy data. In these regions, the earlier versions of the model
602 (Fig. 11a-c) are not even capturing the sign of change and are showing a weak cooling, in stark
603 contrast to the proxy data, that neither HadGEM2 nor HadGEM3 display (Fig. 11d-e). Where proxy
604 data suggest colder conditions, again none of the models are capturing the sign of change and all show
605 widespread warming, and this is most evident in HadGEM3 because of its particularly strong
606 warming. The fact that all of the HadCM3 simulations are showing several regions of cooling and
607 have a higher RMSE than the most recent versions suggests that this early model might be too cold.
608 In contrast, the fact that HadGEM3 has a higher RMSE than HadGEM2 suggests that, despite
609 involving significant model development (see Williams *et al.* 2020 for a summary), concerning
610 Pliocene climate HadGEM3 may actually be too warm. Therefore, whilst model development appears
611 to have improved the model's agreement with proxy data since earlier versions of the model, this only
612 appears to be true up to a certain point; the "sweet spot" appears to be HadGEM2. Moreover, given
613 the aforementioned point about the *mPWP* simulation not being in full equilibrium and being ~1.5°C

614 warmer if it had been (see Section 3.1.2), it is likely that both the SST anomaly and the RMSE values
 615 would be higher when in equilibrium and therefore the performance against proxy data may be lower
 616 than indicated here.

617

618 **4.2. Model-model comparison: HadGEM3 versus PlioMIP2 models**

619 Finally, the focus here is on mean differences, again considering SAT and precipitation anomalies,
 620 between the *mPWP* simulation from HadGEM3 and the Pliocene simulations from all other available
 621 models included in PlioMIP2 (Table 4).

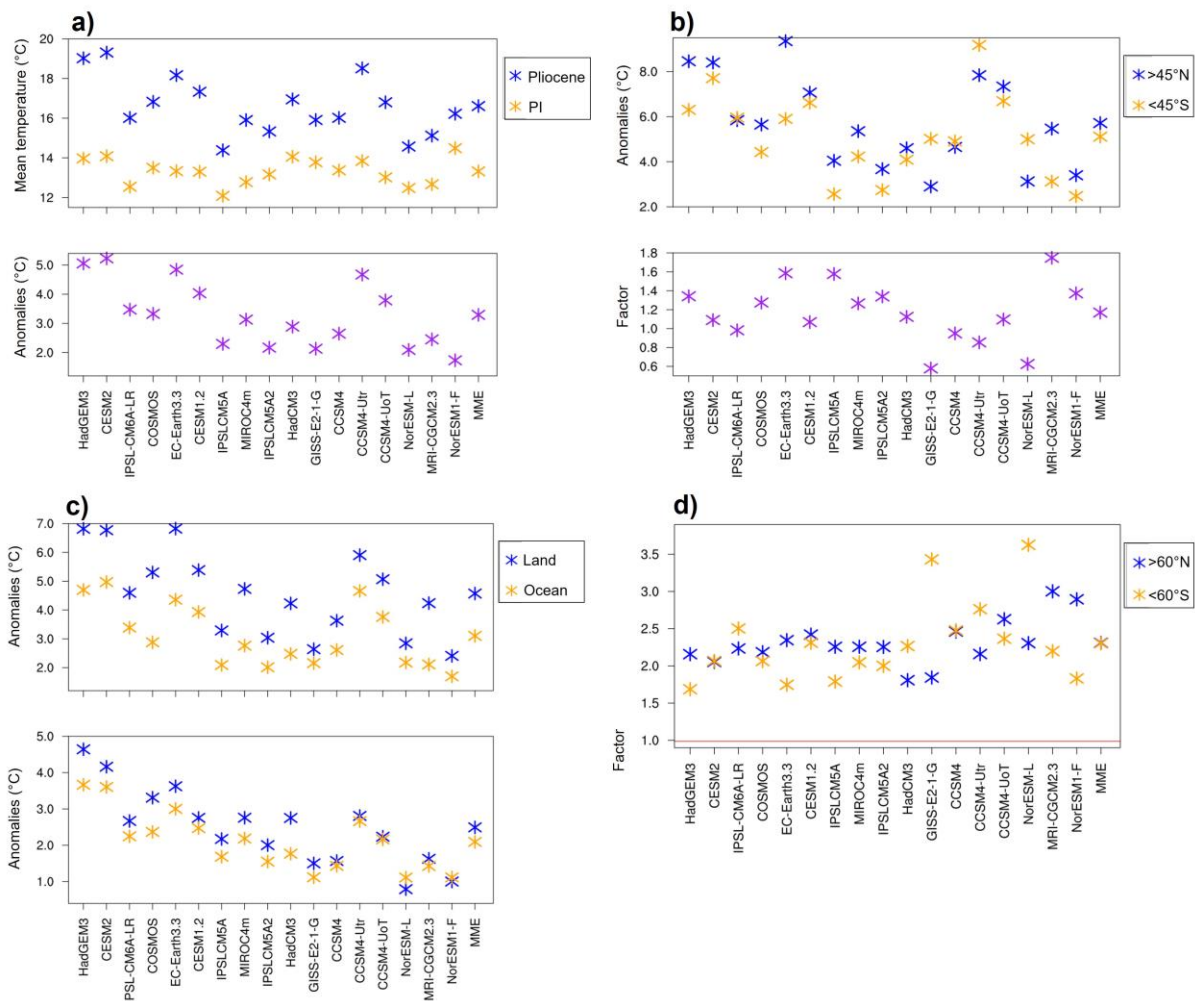
Model, and modelling centre responsible for simulation	Spatial resolution (lon x lat)		ECS (°C)
	Atmosphere	Ocean	
CCSM4, National Centre for Atmospheric Research, US	1° x 1°	1° x 1°	3.2
CCSM4_Utr, Utrecht University, the Netherlands	2.5° x 1.9°	1° x 1°	3.2
CCSM4_UoT, University of Toronto, Canada	1° x 1°	1° x 1°	3.2
CESM1.2, National Centre for Atmospheric Research, US	1° x 1°	1° x 1°	4.1
CESM2, National Centre for Atmospheric Research, US	1° x 1°	1° x 1°	5.3
COSMOS, Alfred Wagner Institute, Germany	3.75° x 3.75°	3.0° x 1.8°	4.7
EC-Earth3.3, Stockholm University, Sweden this	1.125° x 1.125°	1° x 1°	4.3
AGISS-E2-1-G, Goddard Institute for Space Studies, US	2.0° x 2.5°	1.0° x 1.25°	3.3
HadCM3, University of Leeds, UK	2.5° x 3.75°	1.25° x 1.25°	3.5
IPSLCM5A, Laboratoire des Sciences du Climat et de l'Environnement, France	3.75° x 1.9°	2.0° x 2.0°	4.1
IPSLCM5A2, Laboratoire des Sciences du Climat et de l'Environnement, France	3.75° x 1.9°	2.0° x 2.0°	3.6
IPSL-CM6A-LR, Laboratoire des Sciences du Climat et de l'Environnement, France	2.5° x 1.26°	1.0° x 1.0°	4.8
MIROC4m, University of Tokyo, Japan	2.8° x 2.8°	1.4° x 1.4°	3.9
MRI-CGCM2.3, University of Tsukuba, Japan	2.8° x 2.8°	2.0° x 2.0°	2.8

NorESM-L, Bjerknes Centre for Climate Research, Norway	3.75° x 3.75°	3.0° x 3.0°	3.1
NorESM-F, Bjerknes Centre for Climate Research, Norway	1.9° x 2.5°	1.0° x 1.0°	2.3

622
623
624

Table 4 - Climate models included here from PlioMIP2 (see Haywood *et al.* 2020 for each model's reference)

625 A number of different metrics of SAT are shown in Figure 12 for each of the models, as well as the
626 MME; the panels shown here are updated versions of those shown in H20, but now including
627 HadGEM3. It should be noted that, consistent with H20, the models are listed according to their
628 published ECS, with the highest ECS listed first (see Table 4). HadGEM3 has an ECS of 5.5 K
629 (Andrews *et al.* 2019), compared to the 2nd highest model (CESM2) with an ECS of 5.3 K (H20). If,
630 however, all available models within CMIP6 (i.e. not just those having conducted Pliocene
631 simulations) are considered, then HadGEM3 has the 2nd highest ECS, just below that of CanESM5
632 with an ECS of 5.6 K (Zelinka *et al.* 2020).



633
634
635

Figure 12 - SAT from Pliocene simulations from HadGEM3 and all other models in PlioMIP2. a) Global annual mean SAT (top panel) and anomalies (bottom panel); b) Extratropical (+/- 45°) annual mean SAT anomalies (top panel) and ratio (i.e.

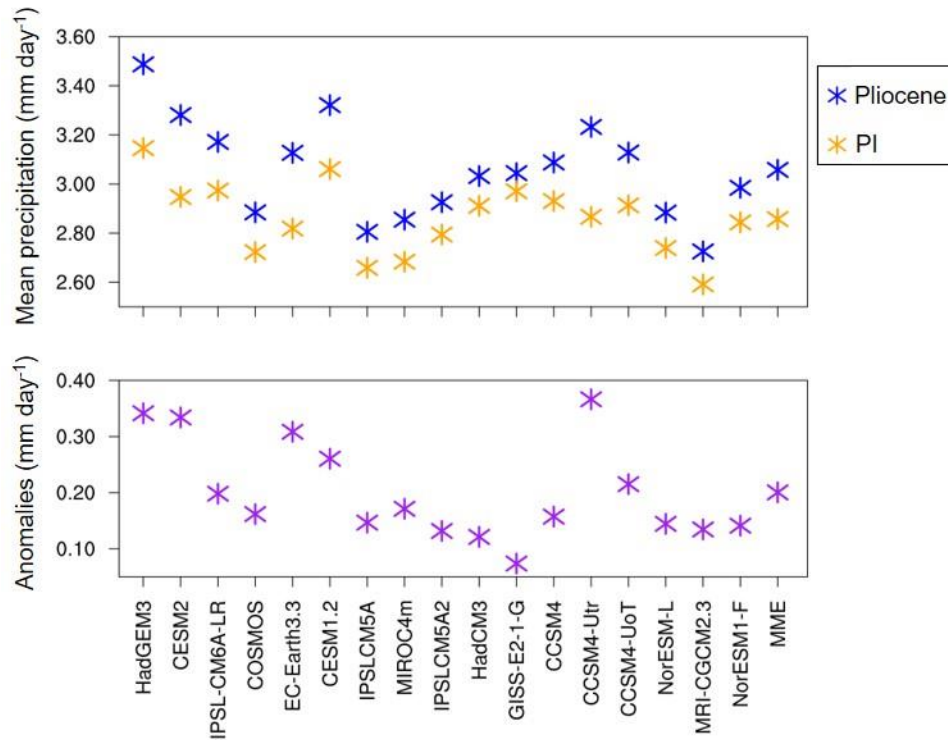
636 >45°N divided by <45°S) between them (bottom panel); c) Land and ocean annual mean SAT anomalies, averaged globally
637 (top panel) and between 20°N-20°S (bottom panel); d) Annual mean SAT polar amplification i.e. SAT poleward of 60°
638 divided by global mean, for each hemisphere, where red line = ratio of 1 (i.e. no polar amplification). Figures reproduced
639 and adapted from Haywood *et al.* (2020)

640

641 As mentioned above (Section 3.2), the global annual SAT anomaly by the end of the *mPWP*
642 simulation is 5.1°C, making HadGEM3 one of the warmest models in PlioMIP2 and second only to
643 CESM2 (H20). This is true both in terms of its anomaly and its mean Pliocene SAT (19°C); this is
644 only lagging behind the warmest model by 0.2°C and 0.3°C for the anomalous and mean SAT,
645 respectively (Fig. 12a). HadGEM3 is much warmer than earlier global annual mean temperature
646 estimates (e.g. Haywood and Valdes 2004), and the range given by models included in PlioMIP1
647 (1.8°C to 3.6°C, see Haywood *et al.* (2013) and PlioMIP2 (1.7°C to 5.2°C, see H20). The impact of
648 including HadGEM3 amongst the models is to increase the MME anomaly by 0.1°C, from 3.2° to
649 3.3°C. Interestingly the HadGEM3 *piControl_mod* simulation is not presenting the warmest absolute
650 PI compared to the other models, coming 4th in the list, suggesting that HadGEM3 is more sensitive to
651 the Pliocene boundary conditions rather than being a generally warmer model overall.

652

653 Concerning annual global mean precipitation (Fig. 13, top panel), as mentioned above the
654 precipitation anomaly by the end of the simulation is 0.34 mm day⁻¹, making HadGEM3 not only one
655 of the warmest models in PlioMIP2 but also one of the wettest (consistent with current understanding,
656 as global precipitation is generally a function of global temperature). The range of anomalies across
657 all models during PlioMIP1 was 0.09 to 0.18 mm day⁻¹ (Haywood *et al.* 2013), during PlioMIP2 it
658 was 0.07 to 0.37 mm day⁻¹ (with the higher values being attributed to the models being more sensitive
659 to the updated PRISM4 boundary conditions) and the PlioMIP2 ensemble mean was 0.19 mm day⁻¹
660 (H20). Concerning the mean, it is the wettest model in terms of both its *mPWP* (3.49 mm day⁻¹) and
661 *piControl_mod* (3.15 mm day⁻¹) simulations, and both of these are much higher than the MME (3.06
662 mm day⁻¹ and 2.86 mm day⁻¹ for the Pliocene and PI simulations, respectively). The fact that both the
663 HadGEM3 *mPWP* and *piControl_mod* simulations are not only the wettest, but are also closer
664 together in terms of mean precipitation, means that if the anomaly is considered (Fig. 13, bottom
665 panel) HadGEM3 is not quite showing the greatest change relative to the PI; an anomaly of 0.34 mm
666 day⁻¹ makes it 2nd only to CCSM4-Utr (at 0.37 mm day⁻¹). The impact of including HadGEM3
667 amongst the other PlioMIP2 models is to again slightly increase the MME anomaly, from 0.19 mm
668 day⁻¹ as reported by H20 to 0.2 mm day⁻¹ here.

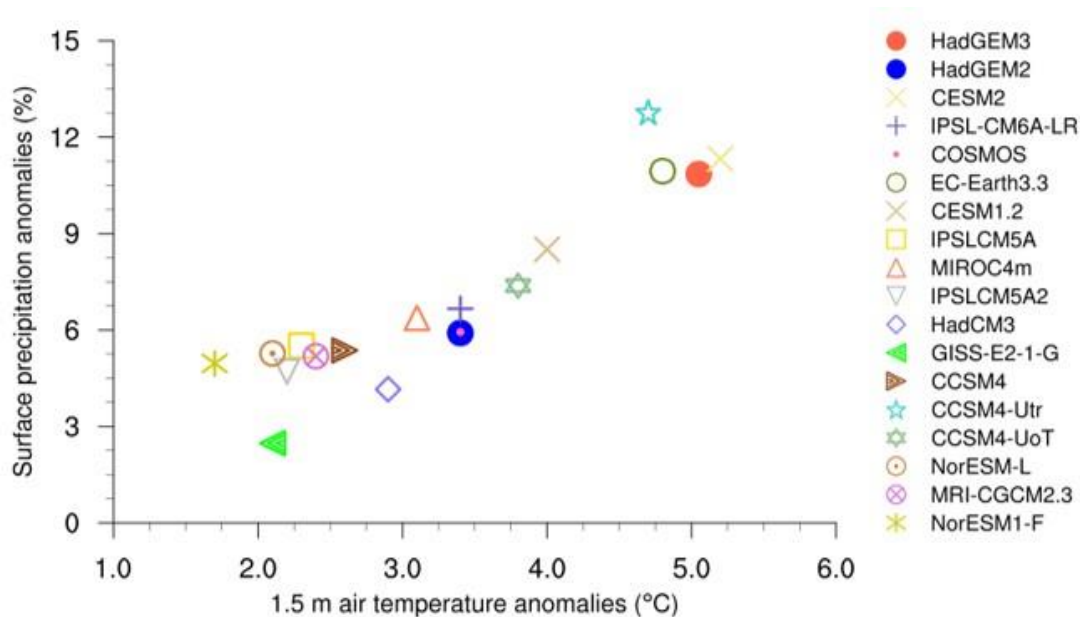


669

670 Figure 13 - Global annual mean surface precipitation (top panel) and anomalies (bottom panel) from HadGEM3 *mPWP*
 671 simulation and all other models in PlioMIP2, as well as multi-model ensemble mean (MME). Figure reproduced and
 672 adapted from Haywood *et al.* (2020)

673

674 If the hydrological sensitivity (i.e. the relationship between global annual mean precipitation
 675 anomalies and SAT anomalies) of the models is considered, then in line with current understanding
 676 (e.g. Pendergrass and Hartmann 2014). there is a clear linear relationship shown by most of the
 677 models, with Pliocene increases in precipitation increasing in line with SAT increases (Fig. 14). This
 678 relationship is not entirely linear, however, with the aforementioned result being shown again here i.e.
 679 although the HadGEM3 *mPWP* simulation is the 2nd warmest of all models in PlioMIP2, it is not the
 680 wettest, suggesting that although the model is highly sensitive to the Pliocene forcings in terms of its
 681 temperature response, it may be less sensitive in terms of its hydrological response.



682
 683 Figure 14 - Global annual mean surface precipitation anomalies (expressed as a percentage) versus global annual mean SAT
 684 from HadGEM3 *mPWP* simulation, HadGEM2 and all other models in PlioMIP2

685
 686 Returning to SAT and if only extratropical warming (separated by hemisphere, above or below 45°N
 687 or S) is considered, then HadGEM3 agrees with the other 11 models (out of 16) that H20 identified as
 688 showing enhanced Northern Hemisphere warming, relative to the Southern Hemisphere (Fig. 12b, top
 689 panel). In the Northern Hemisphere, HadGEM3 is again one of the warmest models and, at 8.46°C, is
 690 considerably warmer than most other models and the MME; this, with the inclusion of HadGEM3, has
 691 now increased from the 5.5°C reported in H20 to 5.7°C here. However, in the Southern Hemisphere
 692 HadGEM3 is closer to many of the other models, albeit still in the top 33% of them, and with a
 693 warming of 6.3°C is much closer to the MME of 5.1°C (Fig. 12b, top panel). This is further
 694 demonstrated by Fig. 12b (bottom panel), showing the ratio of warming between the hemispheres
 695 (calculated by dividing the Northern Hemisphere warming by the Southern Hemisphere warming),
 696 where HadGEM3 is giving a ratio of 1.34 which is again close to many of the other models and the
 697 MME (1.17). Considering land-sea temperature contrasts (Fig. 12c), as H20 state all of the PlioMIP2
 698 models show more warming over land, both globally and across the tropics (defined as 20°N-20°S),
 699 and HadGEM3 is no exception. Indeed, over either land or sea, HadGEM3 is the 2nd warmest
 700 globally and warmest across the tropics, and the inclusion of this model increases the MME by 0.1-
 701 0.14°C depending on whether land or sea warming is considered.

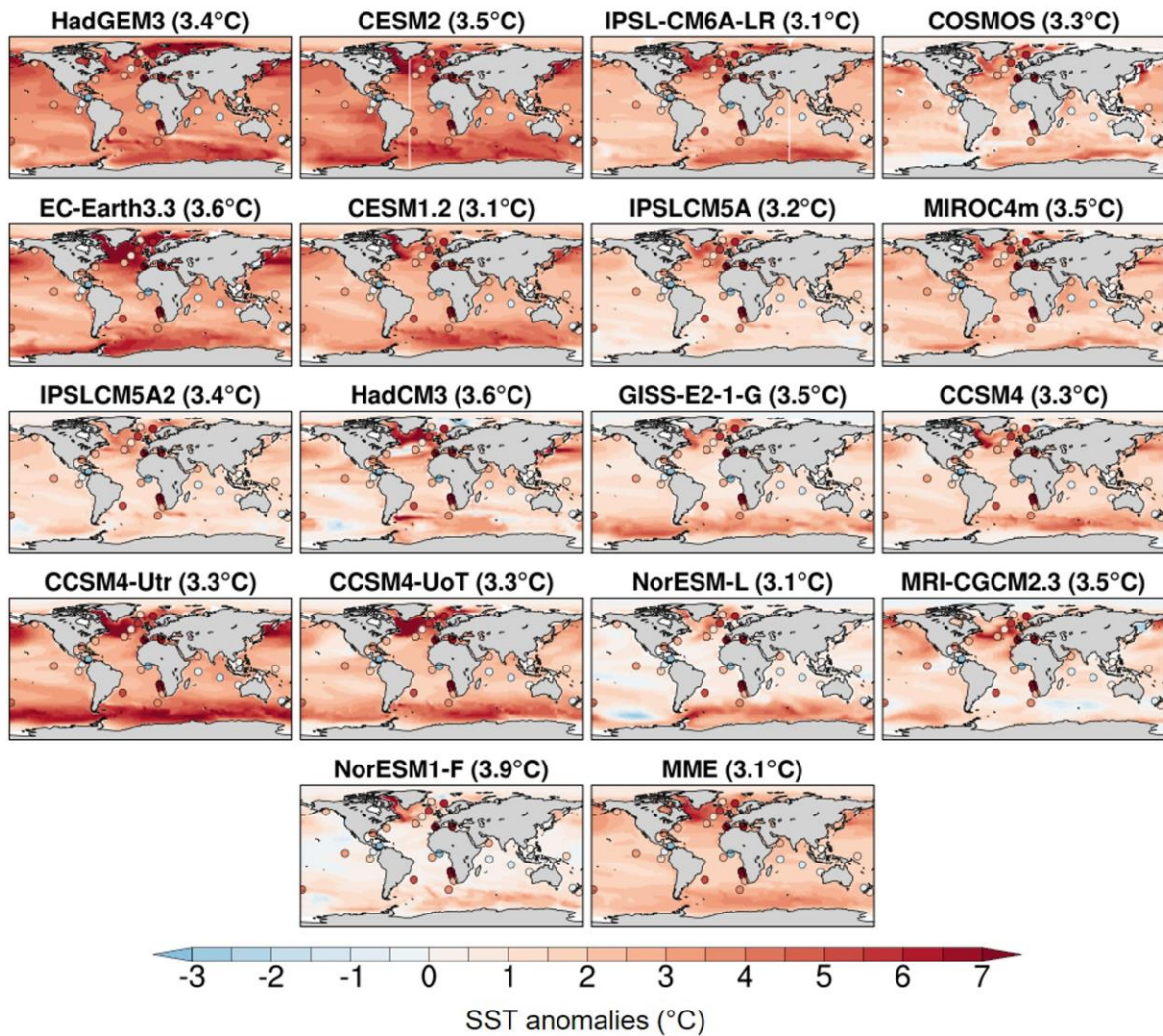
702
 703 HadGEM3 is one of the largest outliers regardless of metric, however concerning polar amplification
 704 this is not the case. Here, as in H20, polar amplification is defined as the ratio of SAT increases
 705 poleward of 60° divided by the global mean SAT increases (Smith *et al.* 2019), calculated
 706 independently for each hemisphere. Despite the HadGEM3 *mPWP* simulation qualitatively showing

707 considerable amplification at both annual and seasonal timescales (Figure 7), when quantitatively
708 compared with all other PlioMIP2 models HadGEM3 is, whilst still having amplification >1 (i.e. that
709 there is some amplification of warming around the poles), nevertheless showing considerably less
710 amplification in both hemispheres, and is also lower than the MME in both hemispheres (Fig. 12d).
711 Of all the models, HadGEM3 comes 4th-to-last for Northern Hemisphere amplification and last for
712 Southern Hemisphere amplification, and its inclusion with the other models reduces the MME ratio by
713 approximately 0.01 and 0.04 for the Northern and Southern Hemisphere, respectively. This is
714 consistent with the conclusions of H20, who note a weak relationship between ECS and amplification;
715 they observe that models with a lower ECS tend to display higher PA, whereas the opposite appears to
716 be shown here i.e. HadGEM3, with one of the highest ECS, is displaying one of the lowest amounts
717 of amplification. The amplification for all the models, as well as the MME, can be seen graphically in
718 Figure S11 in the Supplementary Material where, at first glance, HadGEM3 would appear to be
719 showing one of the largest amounts of amplification. However, and consistent with the observation
720 by H20, this is because the model is showing more warming in the tropics (relative to the other
721 models) rather than less warming at high latitudes.

722

723 Lastly, concerning SST anomalies the HadGEM3 *mPWP* simulation is warmer than most other
724 models in PlioMIP2 (Figure 15). When simulated SST is compared to the proxy data from
725 McClymont *et al.* (2020), if the models are ranked according to RMSE then the HadGEM3 *mPWP*
726 simulation (RMSE = 3.4°C; see Table 3) ranks approximately halfway amongst them. There appears
727 to be a weak relationship between the warmth of the model and agreement with proxy data, with some
728 of the other warm models (e.g. CESM2, the warmest model) showing less agreement (RMSE =
729 3.5°C) with the proxy data than HadGEM3; however, this is not always true, such as the case of the
730 CCSM4-Utr which is also comparatively warm but is showing a slightly better agreement (RMSE =
731 3.3°C) with the proxy data. It is likely that the location of the proxy data is important, as the best
732 agreement comes from the MME (RMSE = 3.1°C) which is showing warm SST anomalies over the
733 North Atlantic and Arctic (better in agreement with the proxy data there) but less warming relative to
734 HadGEM3 and CESM2 in the Southern Hemisphere (better in agreement with the proxy data in e.g.
735 the Indian Ocean).

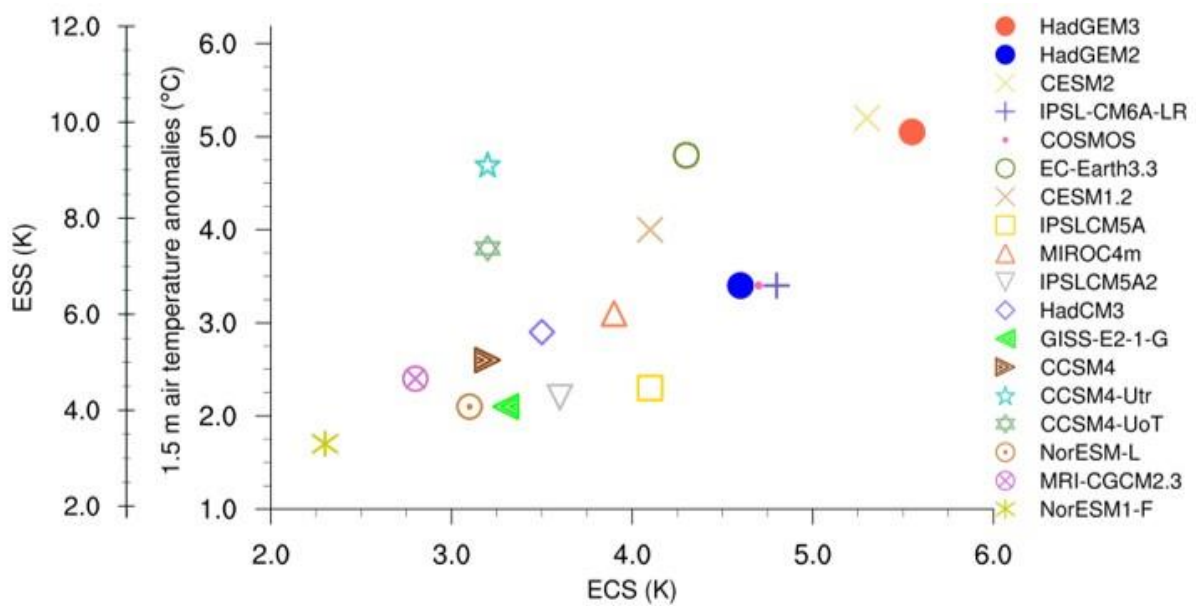
736



737
 738 Figure 15 – SST climatology differences (Pliocene – PI) from HadGEM3 *mPWP* simulation and all other models in
 739 PlioMIP2, as well as multi-model ensemble mean (MME). Numbers in brackets show RMSE scores when compared proxy
 740 data from McClymont *et al.* (2020)

741
 742 It is likely that much of the greater warming in the HadGEM3 *mPWP* simulation, relative to the other
 743 models, can be attributed to the relatively high ECS of this model. Figure 16 shows model ECS
 744 against simulated Pliocene warming for all available models (see Table 4 for individual ECS values).
 745 Also shown on this figure is the Earth System Sensitivity (ESS) which, for the Pliocene, can be taken
 746 as the global mean temperature scaled by the CO₂ forcing for 560 ppmv compared with 400 ppmv.
 747 This is because the temperature change due to the modified orography is small, and so the Pliocene
 748 warming relative to preindustrial is due to the CO₂ forcing and associated feedbacks due to vegetation
 749 and ice sheets, which can be interpreted as ESS (Lunt *et al.* 2010). Therefore, a plot of Pliocene
 750 global mean warming against ECS will be identical to a plot of ESS against ECS, but with different
 751 values on the y axis. There is a clear linear relationship between ECS and global mean warming (or
 752 ESS), with the two models showing the highest ECS also having the highest Pliocene warming or ESS
 753 (HadGEM3 and CESM2). Despite some outliers, such as CCSM4-Utr with a relatively high global

754 mean temperature anomaly but a relatively low ECS, this would suggest that for most models
 755 Pliocene temperature anomalies (and ESS) are increasing in line with ECS.
 756



757
 758 Figure 16 - Global annual mean SAT anomalies versus both ESS (first y-axis) and ECS from HadGEM3 *mPWP* simulation,
 759 HadGEM2 and all other models in PlioMIP2. The ESS axis is calculated by multiplying the global annual mean SAT
 760 anomaly by $\log(560/280)/\log(400/280)$ i.e. by 1.94, meaning the axis here goes from 1.94-11.64 K; for simplicity, this has
 761 been rounded up to 2-12 K
 762

763 **5. SUMMARY AND CONCLUSIONS**

764 This study has introduced the mid-Pliocene simulation using the latest version of the UK’s physical
 765 climate model, HadGEM3-GC31-LL, presented the experimental design and conducted a model-
 766 model and model-data comparison. This study is novel, being the first time this version of the UK
 767 model has been run this far back in time; only two other paleoclimate simulations using this model
 768 have thus far been conducted, comprising the UK’s contribution to CMIP6/PMIP4, and both of these
 769 were more recent, Quaternary simulations (Williams *et al.* 2020).

770
 771 The *mPWP* simulation mostly followed the experimental design defined in H16, with the exception
 772 being the exclusion of a Pliocene LSM and Pliocene soils. Both of these were kept the same as PI.
 773 All other boundary conditions, including CO₂, orography, ice mask, lakes, vegetation fractions and
 774 vegetation functional types followed the protocol of H16, and were incrementally implemented to be
 775 Pliocene, based on the PRISM4 dataset. A minor model parameter change was included to increase
 776 the model’s stability in light of the strong Pliocene forcing, and thus a corresponding PI simulation
 777 was also run for comparison purposes. The *mPWP* simulation was run for 567 years in total, during
 778 which atmospheric and oceanic equilibrium were assessed. Although not meeting the criteria used to
 779 determine equilibrium in other paleoclimate simulations, especially concerning oceanic equilibrium,

780 due to computational restrictions it was not possible to run this model for the thousands of years
781 required to achieve this.

782

783 The results presented here are divided into three sections: i) a simulation comparison, in which the
784 *mPWP* simulation is compared to its corresponding *piControl_mod* simulation (Section 3.2); ii) a
785 model-model and model-data comparison, in which the most recent *mPWP* simulation is compared to
786 Pliocene simulations from previous versions of the same model, all assessed against proxy data
787 (Section 4.1); and iii) a model-model comparison, in which the most recent *mPWP* simulation is
788 compared to other models (Section 4.2).

789

790 For the first comparison, the *mPWP* simulation is behaving in line with current understanding and
791 previous work (e.g. Haywood *et al.* 2013, H20), showing a warmer and wetter world relative to the PI,
792 with the greatest warming occurring over the poles. This polar warming, which can be attributed to a
793 loss in sea ice and changes in clouds, and the changes to precipitation (such as an enhancement of
794 monsoon systems) all agree with the expected response and previous work (e.g. Cronin *et al.* 1993,
795 Howell *et al.* 2016, Li *et al.* 2018, Moran *et al.* 2006, Polyak *et al.* 2010, Zhang *et al.* 2013, 2016).
796 For the second comparison, there is a clear increase in global temperatures (as measured by SST) as
797 the model develops through time, beginning with the early Pliocene simulations using HadCM3 (Lunt
798 *et al.* 2011 and Bragg *et al.* 2012), through HadGEM2 (Tindall and Haywood 2020) and up to the
799 most recent *mPWP* simulation from HadGEM3, presented here. Up to a point, this warming results in
800 a better agreement with available proxy data. However, just as the earlier HadCM3 simulations
801 appear to be too cold relative to some proxy data, the most recent *mPWP* simulation from HadGEM3
802 appears to be too warm; the “sweet spot” appears to be the previous generation of the model,
803 HadGEM2. This would be even more the case had the *mPWP* simulation been allowed to run to full
804 equilibrium, and it is suggested that the final global mean surface temperature could have been
805 approximately 1.5°C higher if so. For the third comparison, the above conclusion that HadGEM3 is
806 too warm is further suggested by the fact that it is one of the warmest and wettest models (even at its
807 current state of equilibrium) in all of PlioMIP2 (H20), and this is true over either land or sea and
808 especially in the Northern Hemisphere. When compared to proxy SST data, HadGEM2 ranks
809 approximately halfway amongst the models, and is much too warm in certain locations, such as the
810 Indian Ocean. However, the conclusion that the model is too warm overall is argued by the fact that
811 the anomalies coming from the HadGEM3 *piControl_mod* simulation are not the warmest, suggesting
812 that rather than the model being too warm in general, the warming may be coming from the model’s
813 sensitivity to the Pliocene forcing. This is consistent with the model’s high ECS, which is among the
814 highest of all the most recent state-of-the-art CMIP6 models (Andrews *et al.* 2019, H20, Zelinka *et al.*
815 2020).

816

817 A number of caveats should be mentioned in this study. The question over the relatively short (but
818 unavoidable due to computational cost) run length has already been discussed, with the results
819 suggesting that the *mPWP* simulation would have been even warmer if it had been allowed to run
820 until true equilibrium. Besides this, firstly any differences to the PlioMIP2 models may be in part
821 related to the fact that the LSM used here is identical to the *piControl*, rather than using the enhanced
822 LSM following the experimental design of H16. This, as discussed above, was necessary, due to
823 technical difficulties in coupling a new LSM to the atmosphere. One of the impacts of this is
824 discussed in Zhang *et al.* (2021), who investigated Atlantic Meridional Overturning Circulation
825 (AMOC) changes during the Pliocene using the PlioMIP2 models. It was found that in contrast to
826 most other PlioMIP2 models, which stimulate a stronger AMOC in the Pliocene relative to the PI,
827 HadGEM3 shows a weaker AMOC, with a maximum of 14.3 Sv and 16.1 Sv for the *mPWP* and
828 *piControl_mod* simulations, respectively (Zhang *et al.* 2021). Secondly, using PI soil parameters and
829 soil dust properties (away from ice regions) may also have an impact on the observed warming;
830 although H16 does provide a set of palaeosol data from Pound *et al.* (2016), this was not used here
831 because of the difficulties in matching the reconstructions to the model's soil-related fields. Thirdly,
832 concerning greenhouse gas forcings, in all of the Pliocene simulations discussed here only CO₂ was
833 modified, with other gases such as methane being left as PI. Given that these trace gases will likely
834 amplify warming, especially in the extratropics (Hopcroft *et al.* 2020), leaving these as PI may be
835 resulting in a cooler climate in all of the simulations. Lastly, the large warming in the *mPWP*
836 simulation may be because certain processes, in particular vegetation, were fixed rather than being
837 interactive (although this is also the case in the majority of the other PlioMIP2 models). In particular,
838 the fact that the introduction of Pliocene vegetation in the *mPWP* simulation results in such a dramatic
839 rise in global SAT (Figure 6) deserves much further exploration. This may be highly important
840 regarding any possible impact on the climate under a Pliocene-style forcing, and therefore current
841 work is underway to investigate the role of vegetation in contributing to the model's simulated
842 warming.

843

844 **DATA AVAILABILITY**

845 Selected fields (SAT, precipitation and SST) from the HadGEM3 *mPWP* simulation are currently
846 available from the Earth System Grid Federation (ESGF) WCRP Coupled Model Intercomparison
847 Project (Phase 6), located at <https://esgf-node.llnl.gov/projects/cmip6/> (last access: 18 March 2021).
848 If other fields are required, they can be made available to the public by directly contacting the lead
849 author. Likewise, access to the other model simulations considered here can be gained by contacting
850 the lead author, or the authors of the appropriate publication (see Haywood *et al.* 2020 for a list of the
851 appropriate publications). For the SST reconstructions, the data can be found within the
852 Supplementary Online Material of
853 McClymont *et al.* (2020), available online at: <https://doi.org/10.5194/cp-16-1599-2020-supplement>.

854

855 **AUTHOR CONTRIBUTIONS**

856 CJRW conducted the *mPWP* simulation, carried out the analysis, produced some of the figures, wrote
857 the majority of the manuscript, and led the paper. XR produced some of the figures. AAS, WHGR,
858 RSS, PH and EJS provided technical assistance in running HadGEM3. JCT, SJH and AMH also
859 provided technical assistance, and contributed the HadGEM2 and HadCM3 simulations. DJL
860 contributed to some of the writing. All authors proofread the paper and provided comments.

861

862 **COMPETING INTERESTS**

863 The authors declare that they have no conflict of interest.

864

865 **ACKNOWLEDGEMENTS**

866 CJRW and DJL acknowledge the financial support of the UK Natural Environment Research Council
867 (NERC)-funded SWEET project, research grant NE/P01903X/1, as well as funding from the
868 European Research Council under the European Union's Seventh Framework Programme (FP/2007-
869 2013)/ERC Grant Agreement no. 340923 (T-GRES). AAS was supported by the Met Office Hadley
870 Centre Climate Programme, funded by BEIS and Defra. XR was supported by the 4D-REEF project,
871 receiving funding from the European Union's Horizon 2020 research and innovation programme
872 under the Marie Skłodowska-Curie research grant, no. 813360. PH was supported by a University of
873 Birmingham Fellowship. RSS was funded by the NERC national capability grant for the UK Earth
874 System Modelling (UKESM) project, research grant NE/N017951/1. AMH and JCT acknowledge
875 receipt of funding from the European Research Council under the European Union's Seventh
876 Framework Programme (FP7/2007-2013)/ERC, grant agreement no. 278636.

877

878 **FINANCIAL SUPPORT**

879 This research has been supported by the NERC-funded SWEET project (grant no. NE/P01903X/1),
880 the Met Office Hadley Centre Climate Programme (funded by BEIS and Defra), the European Union's
881 Horizon 2020 research and innovation programme under the Marie Skłodowska-Curie research grant
882 (no. 813360), a University of Birmingham Fellowship, the NERC UKESM project (grant no.
883 NE/N017951/1) and the European Union's Seventh Framework Programme (FP7/2007-2013)/ERC
884 (grant no. 278636).

885

886 **LIST OF TABLES**

887 Table 1 - Centennial trends (calculated via a linear regression) and climatology in global mean
888 measures of climate equilibrium over the last 50 years of the simulations, adapted from Menary *et al.*
889 (2018) to include the CMIP6 *piControl*, *piControl_mod* and *mPWP* simulations. Negative TOA
890 radiation = net radiation flux is downward

891

892 Table 2 - Different generations of the UK physical climate model used here, and their involvement
893 with PlioMIP

894

895 Table 3 - Global annual mean SST anomalies from Pliocene simulations using different generations of
896 the UK's physical climate model, and RMSE values between simulations and SST proxy data from
897 McClymont *et al.* (2020)

898

899 Table 4 - Climate models included here from PlioMIP2 (see Haywood *et al.* 2020 for each model's
900 reference)

901

902 **LIST OF FIGURES**

903 Figure 1 - Changes to orography in HadGEM3 *mPWP* simulation: a) PRISM4 anomaly; b) Original
904 field used in HadGEM3 *piControl*; c) New field used in HadGEM3 *mPWP*, with smoothed orography
905 over western Antarctica (final version, used in simulation)

906

907 Figure 2 - Ten megabiomes from PlioMIP Phase 2 used create the nine PFTs used in HadGEM3
908 *mPWP* simulation

909

910 Figure 3 - Nine PFTs used in HadGEM3. Top half: *piControl* simulation, bottom half: *mPWP*
911 simulation. Values in brackets show global mean differences (*mPWP* - *piControl*), expressed as a
912 percentage. a) broadleaf trees (18%); b) needle-leaved trees (5%); c) temperate C3 grass (-15%); d)
913 tropical C4 grass (6%); e) shrubs (3%); f) urban areas (no change); g) inland water (1%); h) bare soil
914 (-12%); i) land ice (-5%)

915

916 Figure 4 - LAI used in HadGEM3, for an example PFT (broadleaf trees, January). a) Function used to
917 create LAI, where dashed lines show zonal mean from *piControl* simulation and solid lines show
918 seasonally and latitudinally varying function of this zonal mean; b) example of functional types used
919 in *piControl* simulation; c) same as b) but for the *mPWP* simulation

920

921 Figure 5 – Example of soil-related fields used in HadGEM3. Left-hand column: *piControl*
922 simulation, right-hand column: *mPWP* simulation. First row: Soil parameters (example shows
923 Volumetric soil moisture content at wilting point); Second row: Soil moisture (example shows
924 January, top-level); Third row: Soil temperature (example shows January, top-level). Complete list of
925 fields shown in Supplementary Material Fig. S3 and S4

926

927 Figure 6 – Annual global mean 1.5 m air temperature from the HadGEM3 *mPWP* spin-up phase and
928 production run, as well as the CMIP6 *piControl* and the *piControl_mod*. Labels show introduction of
929 each new Pliocene element. Climatologies discussed here are taken from final 50 years of each
930 simulation (shown by shaded boxes). See Williams *et al.* (2020) for the *piControl* spin-up phase that
931 preceded these simulations.

932

933 Figure 7 – 1.5 m air temperature climatology differences (*mPWP* – *piControl_mod*) from HadGEM3.
934 a) Annual; b) DJF; c) JJA

935

936 Figure 8 – Sea ice fraction climatology differences (*mPWP* – *piControl_mod*) from HadGEM3: a)
937 Northern Hemisphere DJF, b) Northern Hemisphere JJA, c) Southern Hemisphere DJF, d) Southern
938 Hemisphere JJA, e) Mean sea ice area (both absolute values and differences) averaged over either
939 hemisphere

940

941 Figure 9 – Surface precipitation climatology differences (*mPWP* – *piControl_mod*) from HadGEM3.
942 a) Annual; b) DJF; c) JJA

943

944 Figure 10 – Total cloud fraction climatology differences (*mPWP* – *piControl_mod*) from HadGEM3.
945 a) Annual; b) DJF; c) JJA

946

947 Figure 11 – Annual mean SST differences (Pliocene – PI) from different generations of the UK's
948 physical climate model. a) HadCM3-PRISM2; b) HadCM3-PlioMIP2; c) HadCM3-PlioMIP2; d)
949 HadGEM2; e) HadGEM3. Background gridded data shows model simulations, filled circles show
950 SST proxy data from McClymont *et al.* (2020)

951

952 Figure 12 - SAT from Pliocene simulations from HadGEM3 and all other models in PlioMIP2. a)
953 Global annual mean SAT (top panel) and anomalies (bottom panel); b) Extratropical (+/- 45°) annual
954 mean SAT anomalies (top panel) and ratio (i.e. >45°N divided by <45°S) between them (bottom
955 panel); c) Land and ocean annual mean SAT anomalies, averaged globally (top panel) and between
956 20°N-20°S (bottom panel); d) Annual mean SAT polar amplification i.e. SAT poleward of 60°
957 divided by global mean, for each hemisphere, where red line = ratio of 1 (i.e. no polar amplification).
958 Figures reproduced and adapted from Haywood *et al.* (2020)

959

960 Figure 13 - Global annual mean surface precipitation (top panel) and anomalies (bottom panel) from
961 HadGEM3 *mPWP* simulation and all other models in PlioMIP2, as well as multi-model ensemble
962 mean (MME). Figure reproduced and adapted from Haywood *et al.* (2020)

963

964 Figure 14 - Global annual mean surface precipitation anomalies (expressed as a percentage) versus
965 global annual mean SAT from HadGEM3 *mPWP* simulation, HadGEM2 and all other models in
966 PlioMIP2

967

968 Figure 15 – SST climatology differences (Pliocene – PI) from HadGEM3 *mPWP* simulation and all
969 other models in PlioMIP2, as well as multi-model ensemble mean (MME). Numbers in brackets
970 show RMSE scores when compared proxy data from McClymont *et al.* (2020)

971

972 Figure 16 - Global annual mean SAT anomalies versus both ESS (first y-axis) and ECS from
973 HadGEM3 *mPWP* simulation, HadGEM2 and all other models in PlioMIP2. The ESS axis is
974 calculated by multiplying the global annual mean SAT anomaly by $\log(560/280)/\log(400/280)$ i.e. by
975 1.94, meaning the axis here goes from 1.94-11.64 K; for simplicity, this has been rounded up to 2-12
976 K

977

978

979

980

981 **REFERENCES**

982 Andrews, T., Andrews, M. B., Bodas-Salcedo, A., Jones, G. S., Kuhlbrodt, T., Manners, J., Menary,
983 M. B., Ridley, J., Ringer, M. A., Sellar, A. A., Senior, C. A. and Tang, Y.: Forcings, feedbacks, and
984 climate sensitivity in HadGEM3-GC3.1 and UKESM1, JAMES,
985 <https://doi.org/10.1029/2019MS001866>, 2019.

986

987 Best, M. J., Pryor, M., Clark, D. B., Rooney, G. G., Essery, R. L. H., Ménard, C. B., Edwards, J. M.,
988 Hendry, M. A., Gedney, N., Mercado, L. M., Sitch, S., Blyth, E., Boucher, O., Cox, P. M.,
989 Grimmond, C. S. B. And Harding, R. J.: The Joint UK Land Environment Simulator (JULES), model
990 description – Part 1: Energy and water fluxes, *Geosci. Model Dev.*, 4, 677–699,
991 <https://doi.org/10.5194/gmd-4-677-2011>, 2011.

992

993 Berntell, E., Zhang, Q., Li, Q., Haywood, A. M., Tindall, J. C., Hunter, S. J., Zhang, Z., Li, X., Guo,
994 C., Nisancioglu, K. H., Stepanek, C., Lohmann, G., Sohl, L. E., Chandler, M. A., Tan, N., Contoux,
995 C., Ramstein, G., Baatsen, M. L. J., von der Heydt, A. S., Chandan, D., Peltier, W. R., Abe-Ouchi, A.,
996 Chan, W.-L., Kamae, Y., Williams, C. J. R. and Lunt, D. J.: Mid-Pliocene West African Monsoon
997 Rainfall as simulated in the PlioMIP2 ensemble, *Clim. Past Discuss.* [preprint],
998 <https://doi.org/10.5194/cp-2021-16>, in review, 2021.

999

1000 Bragg, F. J., Lunt, D. J. and Haywood, A. M.: Mid-Pliocene climate modelled using the UK Hadley
1001 Centre Model: PlioMIP Experiments 1 and 2, *Geosci. Model Dev.*, 5, 1109-1125, doi:10.5194/gmd-5-
1002 1109-2012, 2012.

1003

1004 Burke, K. D., Williams, J. W., Chandler, M. A., Haywood, A. M., Lunt, D. J. and Otto-Bliesner, B.
1005 L.: Pliocene and Eocene provide best analogs for near-future climates, *PNAS*, 115, 13288-13293,
1006 [10.1073/pnas.1809600115](https://doi.org/10.1073/pnas.1809600115), 2018

1007

1008 Clark, D. B., Mercado, L. M., Sitch, S., Jones, C. D., Gedney, N., Best, M. J., Pryor, M., Rooney, G.
1009 G., Essery, R. L. H., Blyth, E., Boucher, O., Cox, P. M., and Harding, R. J.: The Joint UK Land
1010 Environment Simulator (JULES), model description – Part 2: Carbon fluxes and vegetation, *Geosci.*
1011 *Model Dev.*, 4, 701–722, <https://doi.org/10.5194/gmd-4-701-2011>, 2011.

1012

1013 Cronin, T. M., Whatley, R. C., Wood, A., Tsukagoshi, A., Ikeya, N., Brouwers, E. M., and Briggs, W.
1014 M.: Microfaunal evidence for elevated mid-Pliocene temperatures in the Arctic Ocean,
1015 *Paleoceanography*, 8, 161-173, <https://doi.org/10.1029/93PA00060>, 1993.

1016

1017 Crucifix, M., Betts R. A. and Hewitt, C. D.: Pre-industrial-potential and Last Glacial Maximum global
1018 vegetation simulated with a coupled climate-biosphere model: Diagnosis of bioclimatic relationships,
1019 *Glob. Planet. Chang*, 45 (4), 295-312, DOI: 10.1016/j.gloplacha.2004.10.001, 2005.
1020

1021 Collins, W. J., Bellouin, N., Doutriaux-Boucher, M., Gedney, N., Halloran, P., Hinton, T., Hughes, J.,
1022 Jones, C. D., Joshi, M., Liddicoat, S., Martin, G., O'Connor, F., Rae, J., Senior, C., Sitch, S.,
1023 Totterdell, I., Wiltshire, A., Woodward, S.: Development and evaluation of an Earth-System model-
1024 HadGEM2. *Geosci. Model Dev.* 4, 1051–1075. <https://doi.org/10.5194/gmd-4-1051-2011>, 2011.
1025

1026 Cox, P. M.: Description of the TRIFFID Dynamic Global Vegetation Model - Hadley Centre
1027 Technical Note 24, Met Office, Bracknell, https://jules.jchmr.org/sites/default/files/HCTN_24.pdf,
1028 2001.
1029

1030 Cox, P. M., Betts, R. A., Bunton, C. B., Essery, R. L. H., Rowntree, PR. and Smith, J.: The impact of
1031 new land surface physics on the GCM simulation of climate and climate sensitivity, *Clim. Dyn.*, 15,
1032 183-203, <https://doi.org/10.1007/s003820050276>, 1999.
1033

1034 Delaney, M. L., Be, A. W. H., and Boyle, E. A.: Li, Sr, Mg, and Na in foraminiferal calcite shells
1035 from laboratory culture, sediment traps, and sediment cores, *Geochim. Cosmochim. Ac.*, 49, 1327-
1036 1341, 1985.
1037

1038 Dowsett, H. J.: The PRISM palaeoclimate reconstruction and Pliocene sea-surface temperature, in:
1039 *Deep-Time Perspectives on Climate Change: Marrying the Signal from Computer Models and*
1040 *Biological Proxies*, edited by: Williams, M., Haywood, A. M., Gregory, F. J., and Schmidt, D. N.,
1041 Bath, UK, Geological Soc Publishing House, 459-480, 2007.
1042

1043 Dowsett, H. J., Robinson, M., Haywood, A., Salzmann, U., Hill, D., Sohl, L., Chandler, M., Williams,
1044 M., Foley, K., and Stoll, D.: The PRISM3D paleoenvironmental reconstruction, *Stratigraphy*, 7, 123-
1045 139, 2010.
1046

1047 Dowsett, H., Dolan, A., Rowley, D., Moucha, R., Forte, A. M., Mitrovica, J. X., Pound, M.,
1048 Salzmann, U., Robinson, M., Chandler, M., Foley, K., and Haywood, A.: The PRISM4 (mid-
1049 Piacenzian) paleoenvironmental reconstruction, *Clim. Past*, 12, 1519-1538,
1050 <https://doi.org/10.5194/cp-12-1519-2016>, 2016.
1051

1052 Essery, R. L. H., Best, M. J., Betts, R. A., Cox, P. M., and Taylor, C. M.: Explicit representation of
1053 subgrid heterogeneity in a GCM land surface scheme, *J. Hydrometeor.*, 4, 530–543,
1054 [https://doi.org/10.1175/1525-7541\(2003\)004<0530:EROSHI>2.0.CO;2](https://doi.org/10.1175/1525-7541(2003)004<0530:EROSHI>2.0.CO;2), 2003.
1055

1056 Essery, R. L. H., Best, M. J. and Cox, P. M.: MOSES 2.2 Technical Documentation - Hadley Centre
1057 Technical Note 30, Met Office, Bracknell. https://jules.jchmr.org/sites/default/files/HCTN_30.pdf,
1058 2001.
1059

1060 Foley, K. M. and Dowsett, H. J.: Community sourced mid-Piacenzian sea surface temperature (SST)
1061 data, US Geological Survey data release, <https://doi.org/10.5066/P9YP3DTV>, 2019.
1062

1063 Gregory, J. M., Ingram, W. J., Palmer, M. A., Jones, G. S., Stott, P. A., Thorpe, R. B., Lowe, J. A.,
1064 Johns, T. C. and Williams, K. D.: A new method for diagnosing radiative forcing and climate
1065 sensitivity, *Geophys. Res. Lett.*, 31, L03205, DOI:10.1029/2003GL018747, 2004.
1066

1067 Gordon, C., Cooper, C., Senior, C. A., Banks, H., Gregory, J. M., Johns, T. C., Mitchell, J. F. B., and
1068 Wood, R. A.: The simulation of SST, sea ice extents and ocean heat transports in a version of the
1069 Hadley Centre coupled model without flux adjustments, *Clim. Dynam.*, 16, 147-168, 2000.
1070

1071 Hardiman, S. C., Andrews, M. B., Andrews, T., Bushell, A. C., Dunstone, N. J., Dyson, H., Jones, G.
1072 S., Knight, J. R., Neinger, E., O'Connor, F. M., Ridley, J. K., Ringer, M. A., Scaife, A. A., Senior,
1073 C. A. and Wood, R. A.: The impact of prescribed ozone in climate projections run with HadGEM3-
1074 GC3.1, *JAMES*, 11, <https://doi.org/10.1029/2019MS001714>, 2019.
1075

1076 Harrison, S. P. and Prentice, I. C.: Climate and CO₂ controls on global vegetation distribution at the
1077 last glacial maximum: analysis based on palaeovegetation data, biome modelling and palaeoclimate
1078 simulations, *Glob. Change Bio.*, 9 (7), 983-1004, <https://doi.org/10.1046/j.1365-2486.2003.00640.x>,
1079 2003.
1080

1081 Haywood, A. M., Dowsett, H. J., Dolan, A. M., Rowley, D., Abe-Ouchi, A., Otto-Bliesner, B.,
1082 Chandler, M. A., Hunter, S. J., Lunt, D. J., Pound, M., and Salzmann, U.: The Pliocene Model
1083 Intercomparison Project (PlioMIP) Phase 2: scientific objectives and experimental design, *Clim. Past*,
1084 12, 663–675, <https://doi.org/10.5194/cp-12-663-2016>, 2016
1085

1086 Haywood, A. M., Hill, D. J., Dolan, A. M., Otto-Bliesner, B. L., Bragg, F., Chan, W.-L., Chandler, M.
1087 A., Contoux, C., Dowsett, H. J., Jost, A., Kamae, Y., Lohmann, G., Lunt, D. J., Abe-Ouchi, A.,
1088 Pickering, S. J., Ramstein, G., Rosenbloom, N. A., Salzmann, U., Sohl, L., Stepanek, C., Ueda, H.,

1089 Yan, Q., and Zhang, Z.: Large-scale features of Pliocene climate: results from the Pliocene Model
1090 Intercomparison Project, *Clim. Past*, 9, 191-209, <https://doi.org/10.5194/cp-9-191-2013>, 2013
1091

1092 Haywood, A. M., Tindall, J. C., Dowsett, H. J., Dolan, A. M., Foley, K. M., Hunter, S. J., Hill, D. J.,
1093 Chan, W.-L., Abe-Ouchi, A., Stepanek, C., Lohmann, G., Chandan, D., Peltier, W. R., Tan, N.,
1094 Contoux, C., Ramstein, G., Li, X., Zhang, Z., Guo, C., Nisancioglu, K. H., Zhang, Q., Li, Q., Kamae,
1095 Y., Chandler, M. A., Sohl, L. E., Otto-Bliesner, B. L., Feng, R., Brady, E. C., von der Heydt, A. S.,
1096 Baatsen, M. L. J. and Lunt, D. J.: The Pliocene Model Intercomparison Project Phase 2: large-scale
1097 climate features and climate sensitivity, *Clim. Past*, 16, 2095-2123, [https://doi.org/10.5194/cp-16-](https://doi.org/10.5194/cp-16-2095-2020)
1098 [2095-2020](https://doi.org/10.5194/cp-16-2095-2020), 2020.
1099

1100 Haywood, A. M. and Valdes, P. J.: Modelling Middle Pliocene warmth: contribution of atmosphere,
1101 oceans and cryosphere, *Earth Planet. Sc. Lett.*, 218, 363–377, doi:10.1016/S0012-821X(03)00685-X,
1102 2004.
1103

1104 Hunter, S. J., Haywood, A. M., Dolan, A. M. and Tindall, J. C.: The HadCM3 contribution to PlioMIP
1105 phase 2, *Clim. Past*, 15, 1691-1713, <https://doi.org/10.5194/cp-15-1691-2019>, 2019.
1106

1107 Hopcroft, P. O., Ramstein, G., Pugh, T.A.M., Hunter, S. J., Murguia-Flores, F., Quiquet, A., Sun, Y.,
1108 Tan, N. and Valdes, P. J.: Polar amplification of Pliocene climate by elevated trace gas radiative
1109 forcing, *Proceedings of the National Academy of Sciences*, DOI: 10.1073/pnas.2002320117, 2020
1110

1111 Howell, F. W., Haywood, A. M., Otto-Bliesner, B. L., Bragg, F., Chan, W.-L., Chandler, M. A.,
1112 Contoux, C., Kamae, Y., Abe-Ouchi, A., Rosenbloom, N. A., Stepanek, C., and Zhang, Z.: Arctic sea
1113 ice simulation in the PlioMIP ensemble, *Clim. Past*, 12, 749-767, [https://doi.org/10.5194/cp-12-749-](https://doi.org/10.5194/cp-12-749-2016)
1114 [2016](https://doi.org/10.5194/cp-12-749-2016), 2016.
1115

1116 Knutti, R. and Rugenstein, M. A. A.: Feedbacks, climate sensitivity and the limits of linear models,
1117 *Phil. Trans. R. Soc. A*, 373, 20150146, <http://dx.doi.org/10.1098/rsta.2015.0146>, 2015.
1118

1119 Kuhlbrodt, T., Jones, C. G., Sellar, A. et al.: The low resolution version of HadGEM3 GC3.1:
1120 Development and evaluation for global climate, *JAMES*, 10: 2865-2888,
1121 <https://doi.org/10.1029/2018MS001370>, 2018.
1122

1123 Li, X. Y., Jiang, D. B., Tian, Z. P., and Yang, Y. B.: Mid-Pliocene
1124 global land monsoon from PlioMIP1 simulations, *Palaeogeogr. Palaeoclimatol.*, 512, 56-70,
1125 <https://doi.org/10.1016/j.palaeo.2018.06.027>, 2018.

1126
1127 Lunt, D. J., Bragg, F., Chan, W.-L., Hutchinson, D. K., Ladant, J.-B., Morozova, P., Niezgodzki, I.,
1128 Steinig, S., Zhang, Z., Zhu, J., Abe-Ouchi, A., Anagnostou, E., de Boer, A. M., Coxall, H. K.,
1129 Donnadieu, Y., Foster, G., Inglis, G. N., Knorr, G., Langebroek, P. M., Lear, C. H., Lohmann, G.,
1130 Poulsen, C. J., Sepulchre, P., Tierney, J. E., Valdes, P. J., Volodin, E. M., Dunkley Jones, T., Hollis,
1131 C. J., Huber, M. and Otto-Bliesner, B. L.: DeepMIP: model intercomparison of early Eocene climatic
1132 optimum (EECO) large-scale climate features and comparison with proxy data, *Clim. Past*, 17, 203-
1133 227, <https://doi.org/10.5194/cp-17-203-2021>, 2021.
1134
1135 Lunt, D. J., Haywood, A. M., Schmidt, G. A., Salzmann, U., Valdes, P. J. and Dowsett, H. J.: Earth
1136 system sensitivity inferred from Pliocene modelling and data, *Nature Geoscience*, 3, 60-64,
1137 DOI:10.1038/ngeo706, 2010.
1138
1139 Lunt, D. J., Haywood, A. M., Schmidt, G. A., Salzmann, U., Valdes, P. J., Dowsett, H. J. and
1140 Loptson, C. A.: On the causes of mid-Pliocene warmth and polar amplification, *EPSL*, 321-322, 128-
1141 138, doi:10.1016/j.epsl.2011.12.042, 2012
1142
1143 Lunt, D. J., Huber, M., Anagnostou, E., Baatsen, M. L. J., et al.: The DeepMIP contribution to
1144 PMIP4: experimental design for model simulations of the EECO, PETM, and pre-PETM (version
1145 1.0), *Geosci. Model Dev.*, 10, 889-901, doi:10.5194/gmd-10-889-2017, 2017.
1146
1147 Martin, G. M. et al.: The HadGEM2 family of Met Office Unified Model climate configurations.
1148 *Geosci. Model Dev.* 4, 723-757. <https://doi.org/10.5194/gmd-4-723-2011>, 2011.
1149
1150 McClymont, E. L., Ford, H. L., Ho, S. L., Tindall, J. C., Haywood, A. M., Alonso-Garcia, M., Bailey,
1151 I., Berke, M. A., Littler, K., Patterson, M. O., Petrick, B., Peterse, F., Ravelo, A. C., Risebrobakken,
1152 B., De Schepper, S., Swann, G. E. A., Thirumalai, K., Tierney, J. E., van der Weijst, C., White, S.,
1153 Abe-Ouchi, A., Baatsen, M. L. J., Brady, E. C., Chan, W.-L., Chandan, D., Feng, R., Guo, C., von der
1154 Heydt, A. S., Hunter, S., Li, X., Lohmann, G., Nisancioglu, K. H., Otto-Bliesner, B. L., Peltier, W. R.,
1155 Stepanek, C. and Zhang, Z.: Lessons from a high-CO₂ world: an ocean view from ~ 3 million years
1156 ago, *Clim. Past*, 16, 1599–1615, <https://doi.org/10.5194/cp-16-1599-2020>, 2020.
1157
1158 Menary, M. B., Kuhlbrodt, T., Ridley, J. et al.: Pre-industrial control simulations with HadGEM3-
1159 GC3.1 for CMIP6, *JAMES*, 10: 3049–3075, <https://doi.org/10.1029/2018MS001495>, 2018.
1160
1161 Moran, K., Backman, J., Brinkhuis, H., et al.: The Cenozoic palaeoenvironment of the Arctic Ocean,
1162 *Nature*, 441, 601-605, <https://doi.org/10.1038/nature04800>, 2006.

1163
1164 Pendergrass, A. and Hartmann, D. L.: Changes in the distribution of rain frequency and intensity in
1165 response to global warming, *J. Clim.*, 27, 8372-8383, DOI:10.1175/JCLI-D-14-00183.1, 2014.
1166
1167 Polyak, L., Alley, R. B., Andrews, J. T., Brigham-Grette, J., Cronin, T. M., Darby, D. A., Dyke, A. S.,
1168 Fitzpatrick, J. J., Funder, S., Holland, M., Jennings, A. E., Miller, G. H., O'Regan, M., Savelle, J.,
1169 Serreze, M., St. John, K., White, J. W. C., and Wolff, E.: History of sea-ice in the Arctic, *Quaternary*
1170 *Sci. Rev.*, 29, 1757-1778, doi:10.1016/j.quascirev.2010.02.010, 2010.
1171
1172 Pound, M. J., Tindall, J., Pickering, S. J., Haywood, A. M., Dowsett, H. J., and Salzmann, U.: Late
1173 Pliocene lakes and soils: a global data set for the analysis of climate feedbacks in a warmer world,
1174 *Clim. Past*, 10, 167-180, <https://doi.org/10.5194/cp-10-167-2014>, 2014.
1175
1176 Prah, F. G. and S. G. Wakeham: Calibration of unsaturation patterns in long-chain ketone
1177 compositions for palaeotemperature assessment, *Nature*, 320, 367-369, 1987.
1178
1179 Ridley, J., Blockley, E., Keen, A. B. et al.: The sea ice model component of HadGEM3-GC3.1, *GMD*,
1180 11: 713-723, <https://doi.org/10.5194/gmd-11-713-2018>, 2017
1181
1182 Siahhan, A., and Walton, J.: The low resolution version of HadGEM3 GC3.1: Development and
1183 evaluation for global climate, *JAMES*, 10, 2865-2888, <https://doi.org/10.1029/2018MS001370>, 2018.
1184
1185 Salzmann, U., Dolan, A. M., Haywood, A. M., Chan, W.-L., Voss, J., Hill, D., Abe-Ouchi, A., Otto-
1186 Bliesner, B., Bragg, F. J., Chandler, M. A., Contoux, C., Dowsett, H. J., Jost, A., Kamae, Y.,
1187 Lohmann, G., Lunt, D. J., Pickering, S. J., Pound, M. J., Ramstein, G., Rosenbloom, N. A., Sohl, L.,
1188 Stepamek, C., Ueda, H. and Zhang, Z.: Challenges in quantifying Pliocene terrestrial warming
1189 revealed by data-model discord, *Nat. Clim. Chang.*, 3, 969-974, <https://doi.org/10.1038/nclimate2008>,
1190 2013.
1191
1192 Salzmann, U., Haywood, A. M., Lunt, D. J., Valdes, P. J. and Hill, D. J.: A new global biome
1193 reconstruction and data-model comparison for the Middle Pliocene, *Global Ecol. Biogeogr.*, 17, 432-
1194 447, <https://doi.org/10.1111/j.1466-8238.2008.00381.x>, 2008.
1195
1196 Sellar, A. A., Jones, C. G., Mulcahy, J. P., Tang, Y., Yool, A., Wiltshire, A., et al.: UKESM1:
1197 Description and evaluation of the U.K. Earth System Model, *JAMES*, 11,
1198 <https://doi.org/10.1029/2019MS001739>, 2019.
1199

1200 Sellar, A. A., Walton, J., Jones, C. G., Wood, R., et al.: Implementation of U.K. Earth System Models
1201 for CMIP6, JAMES, 12, <https://agupubs.onlinelibrary.wiley.com/doi/full/10.1029/2019MS001946>,
1202 2020.

1203

1204 Smith, D. M., Screen, J. A., Deser, C., Cohen, J., Fyfe, J. C., García-Serrano, J., Jung, T., Kattsov, V.,
1205 Matei, D., Msadek, R., Peings, Y., Sigmond, M., Ukita, J., Yoon, J.-H., and Zhang, X.: The Polar
1206 Amplification Model Intercomparison Project (PAMIP) contribution to CMIP6: investigating the
1207 causes and consequences of polar amplification, GMD, 12, 1139-1164, [https://doi.org/10.5194/gmd-](https://doi.org/10.5194/gmd-12-1139-2019)
1208 12-1139-2019, 2019.

1209

1210 Storkey, D., Megann, A., Mathiot, P. et al.: UK Global Ocean GO6 and GO7: A traceable hierarchy
1211 of model resolutions, GMD, 11: 3187-3213, <https://doi.org/10.5194/gmd-11-3187-2018>, 2017
1212

1213 Tierney, J. E., Poulsen, C. J., Montañez, I. P., Bhattacharya, T., Feng, R., Ford, H. L., Hönlisch, B.,
1214 Inglis, G. N., Petersen, S. V., Sagoo, N., Tabor, C. R., Thirumalai, K., Zhu, J., Burls, N. J., Foster, G.
1215 L., Goddérís, Y., Huber, B. T., Ivany, L. C., Turner, S. K., Lunt, D. J., McElwain, J. C., Mills, B. J.
1216 W., Otto-Bliesner, B. L., Ridgwell, A. and Zhang, Y. G.: Past climates inform our future, Science,
1217 370, 6517, eaay3701, DOI:10.1126/science.aay3701, 2020.

1218

1219 Tindall, J. C. and Haywood, A. M.: Modelling the mid-Pliocene warm period using HadGEM2, Glob.
1220 Planet. Chang, 186, <https://doi.org/10.1016/j.gloplacha.2019.103110>, 2020.

1221

1222 Valdes, P. J., Armstrong, E., Badger, M. P. S., Bradshaw, C. D., Bragg, F., Crucifix, M., Davies-
1223 Barnard, T., Day, J. J., Farnsworth, A., Gordon, C., Hopcroft, P. O., Kennedy, A. T., Lord, N. S.,
1224 Lunt, D. J., Marzocchi, A., Parry, L. M., Pope, V., Roberts, W. H. G., Stone, E. J., Tourte, G. J. L.,
1225 and Williams, J. H. T.: The BRIDGE HadCM3 family of climate models: HadCM3@Bristol v1.0,
1226 Geosci. Model Dev., 10, 3715-3743, <https://doi.org/10.5194/gmd-10-3715-2017>, 2017.

1227

1228 Walters, D., Baran, A. J., Boutle, I., Brooks, M., Earnshaw, P., Edwards, J., Furtado, K., Hill, P.,
1229 Lock, A., Manners, J., Morcrette, C., Mulcahy, J., Sanchez, C., Smith, C., Stratton, R., Tennant, W.,
1230 Tomassini, L., Van Weverberg, K., Vosper, S., Willett, M., Browse, J., Bushell, A., Carslaw, K.,
1231 Dalvi, M., Essery, R., Gedney, N., Hardiman, S., Johnson, B., Johnson, C., Jones, A., Jones, C.,
1232 Mann, G., Milton, S., Rumbold, H., Sellar, A., Ujiie, M., Whitall, M., Williams, K., and Zerroukat,
1233 M.: The Met Office Unified Model Global Atmosphere 7.0/7.1 and JULES Global Land 7.0
1234 configurations, Geosci. Model Dev., 12, 1909-1963, <https://doi.org/10.5194/gmd-12-1909-2019>,
1235 2019.

1236

1237 Williams, C. J. R., Guarino, M.-V., Capron, E., Malmierca-Vallet, I., Singarayer, J. S., Sime, L. C.,
1238 Lunt, D. J., and Valdes, P. J.: CMIP6/PMIP4 simulations of the mid-Holocene and Last Interglacial
1239 using HadGEM3: comparison to the pre-industrial era, previous model versions and proxy data, *Clim.*
1240 *Past*, 16, 1429-1450, <https://doi.org/10.5194/cp-16-1429-2020>, 2020.

1241

1242 Williams, K. D., Copsey, D., Blockley, E. W., Bodas-Salcedo, A., Calvert, D., Comer, R., Davis, P.,
1243 Graham, T., Hewitt, H. T., Hill, R., Hyder, P., Ineson, S., Johns, T. C., Keen, A. B., Lee, R. W.,
1244 Megann, A., Milton, S. F., Rae, J. G. L., Roberts, M. J., Scaife, A. A., Schiemann, R., Storkey, D.,
1245 Thorpe, L., Watterson, I. G., Walters, D. N., West, A., Wood, R. A., Woollings, T., and Xavier, P. K.:
1246 The Met Office Global Coupled Model 3.0 and 3.1 (GC3.0 and GC3.1) Configurations, *JAMES*, 10,
1247 357-380, <https://doi.org/10.1002/2017MS001115>, 2017.

1248

1249 Zelinka, M. D., Myers, T. A., McCoy, D. T., Po-Chedley, S., Caldwell, P. M., Ceppi, P., Klein, S. A.
1250 and Taylor, K. E.: Causes of higher climate sensitivity in CMIP6 models, *Geophys. Res. Lett.*, 47,
1251 e2019GL085782. <https://doi.org/10.1029/2019GL085782>, 2020.

1252

1253 Zhang, R., Yan, Q., Zhang, Z. S., Jiang, D., Otto-Bliesner, B. L., Haywood, A. M., Hill, D. J., Dolan,
1254 A. M., Stepanek, C., Lohmann, G., Contoux, C., Bragg, F., Chan, W.-L., Chandler, M. A., Jost, A.,
1255 Kamae, Y., Abe-Ouchi, A., Ramstein, G., Rosenbloom, N. A., Sohl, L., and Ueda, H.: Mid-Pliocene
1256 East Asian monsoon climate simulated in the PlioMIP, *Clim. Past*, 9, 2085-2099,
1257 <https://doi.org/10.5194/cp-9-2085-2013>, 2013.

1258

1259 Zhang, R., Zhang, Z. S., Jiang, D. B., Yan, Q., Zhou, X., and Cheng, Z. G.: Strengthened African
1260 summer monsoon in the mid-Piacenzian, *Adv. Atmos. Sci.*, 33, 1061-1070,
1261 <https://doi.org/10.1007/s00376-016-5215-y>, 2016.

1262

1263 Zhang, Z., Li, X., Guo, C., Otterå, O. H., Nisancioglu, K. H., Tan, N., Contoux, C., Ramstein, G.,
1264 Feng, R., Otto-Bliesner, B. L., Brady, E., Chandan, D., Peltier, W. R., Baatsen, M. L. J., von der
1265 Heydt, A. S., Weiffenbach, J. E., Stepanek, C., Lohmann, G., Zhang, Q., Li, Q., Chandler, M. A.,
1266 Sohl, L. E., Haywood, A. M., Hunter, S. J., Tindall, J. C., Williams, C. J. R., Lunt, D. J., Chan, W.-L.
1267 and Abe-Ouchi, A.: Mid-Pliocene Atlantic Meridional Overturning Circulation simulated in
1268 PlioMIP2, *Clim. Past*, 17, 529-543, <https://doi.org/10.5194/cp-17-529-2021>, 2021.

1269

1270 Zhu, J., Poulsen, C. J. and Otto-Bliesner, B. L.: High climate sensitivity in CMIP6 model not
1271 supported by paleoclimate, *Nat. Clim. Chang.*, 10, 378-379, [https://doi.org/10.1038/s41558-020-0764-](https://doi.org/10.1038/s41558-020-0764-6)
1272 [6](https://doi.org/10.1038/s41558-020-0764-6), 2020.

1273

1274

1275

1276